Redox Biology 69 (2024) 103010

Contents lists available at ScienceDirect

Redox Biology

journal homepage: www.elsevier.com/locate/redox

Empagliflozin improves mitochondrial dysfunction in diabetic cardiomyopathy by modulating ketone body metabolism and oxidative stress

Weijuan Cai [a], Kunying Chong [b], Yunfei Huang [c], Chun Huang [c], Liang Yin [c,*]

[a] Institute of Clinical Medicine, Central People's Hospital of Zhanjiang, Zhanjiang, 524000, China
[b] Department of Endocrinology and Metabolism, Affiliated Hospital of Qingdao Binhai University, Qingdao, 266404, China
[c] Department of Endocrinology and Metabolism, Central People's Hospital of Zhanjiang, Zhanjiang, 524000, China

ARTICLE INFO

Keywords:
Diabetic cardiomyopathy
SGLT2 inhibitor
Ketone body metabolism
Oxidative stress
Mitochondrial dysfunction

ABSTRACT

Ketone bodies are considered as an alternative energy source for diabetic cardiomyopathy (DCM) and can improve the energy supply of the heart muscle, suggesting that it may be an important area of research and development as a therapeutic target for DCM. Cumulative cardiovascular trials have shown that sodium-glucose cotransporter 2 (SGLT2) inhibitors reduce cardiovascular events in diabetic populations. Whether SGLT2 inhibitors improve DCM by enhancing ketone body metabolism remains and whether they help prevent oxidative damage remains to be clarified. Here, we present the combined results of nine GSE datasets for diabetic cardiomyopathy (GSE215979, GSE161931, GSE145294, GSE161052, GSE173384, GSE123975, GSE161827, GSE210612, and GSE5606). We found significant up-regulated gene 3-hydroxymethylglutaryl CoA synthetase 2 (HMGCS2) and down-regulated gene 3-hydroxybutyrate dehydrogenase (BDH1) and 3-oxoacid CoA-transferase1 (OXCT1), respectively. Based on the analysis of the constructed protein interaction network, it was found that HMGCS2 was in the core position of the interaction network. In addition, Gene ontology (GO) enrichment analysis mainly focused on redox process, acyl-CoA metabolic process, catalytic activity, redox enzyme activity and mitochondria. The activity of HMGCS2 in DCM heart was increased, while the expression of ketolysis enzymes BDH1 and OXCT1 was inhibited. In vivo, Empagliflozin (Emp) treated DCM group significantly decreased ventricular weight, myocardial cell cross-sectional area, and myocardial fibrosis. In addition, Emp further promoted the activity of BDH1 and OXCT1, increased the utilization of ketone bodies, further promoted the activity of HMGCS2 in DCM, and increased the synthesis of ketone bodies, prevented mitochondrial breakage and dysfunction, increased myocardial ATP to provide sufficient energy, inhibited oxidative stress and apoptosis of cardiac cells ex vivo, and improved the myocardial dysfunction of DCM. Emp can improve mitochondrial dysfunction in diabetic cardiomyopathy by regulating ketone body metabolism and oxidative stress. These findings provide a theoretical basis for evaluating Emp as a treatment for DCM.

1. Introduction

Diabetic cardiomyopathy (DCM) is a specific heart disease caused by diabetes, independent of other cardiovascular diseases [1]. The heart is an organ with high energy requirements and metabolic flexibility, so it can produce a variety of energy substrates to produce ATP under different physiological conditions. Impaired metabolic balance and oxidative stress damage have been shown to be an important aspect of DCM. Therefore, maintaining cardiometabolic homeostasis is a promising strategy for the treatment of DCM.

Ketone bodies have been shown to be an alternative energy source for heart failure, which can improve myocardial energy supply and thus adapt to heart failure. The traditional view is that ketone bodies are only produced in the liver [2]. However, in recent years, it has also been found that ketone bodies are produced in tumor cells [3], heart [4], kidney [5], central nervous system [6,7], islet beta cells [8] and retinal pigment epithelial cells [9]. Recent studies have reported changes in the expression level of the ketogenic rate-limiting enzyme 3-hydroxymethylglutaryl CoA synthetase 2 (HMGCS2) in DCM [10,11]. In addition, decreased ketone body oxidation was found in the hearts of db/db mice [12]. Other study has also shown that decreased myocardial

* Corresponding author. Department of Endocrinology and Metabolism, Central People's Hospital of Zhanjiang, 236 Yuanzhu Road, Zhanjiang, 524000, China.
E-mail address: cwj_yl@163.com (L. Yin).

https://doi.org/10.1016/j.redox.2023.103010
Received 26 November 2023; Received in revised form 18 December 2023; Accepted 21 December 2023
Available online 27 December 2023

Abbreviations

3-NT	3-nitrotyrosine
4-HNE	4-hydroxy-2-nonenal
AcAc	Acetoacetate
ACOT1	Acyl-CoA thioesterase 1
ANOVA	One-way analysis of variance
ANP	Atrial natriuretic peptide
BDH1	3-hydroxybutyrate dehydrogenase
BKs	C57BLKs
β-OHB	β-hydroxybutyrate
BP	Biological process
Ctrl/CTR/CON	Control
CAT	Catalase
CC	Cellular component
CD	Control diet
CK	Control check
DAB	Diaminobenzidine
DAPA-HF	Dapagliflozin and Prevention of Advers e Outcomes in Heart Failure
DAPI	4′, 6-diamidino-2-phenylindole
DAVID	Database for Annotation, Visualization and Integrated Discovery
DCM	Diabetic cardiomyopathy
DEGs	Differential expression genes
DM	Ddiabetes mellitus
DRP1	Dynamin-associated protein 1
ECL	Enhanced chemiluminescence
ELISA	Enzyme-linked immunosorbent assay
Emp	Empagliflozin
ETC	Electron transport chain
EMPEROR Reduced	Empagliflozin Outcome Trial in Patient s with Chronic Heart Failure and a Reduced Ejection Fraction
GEO	Gene Expression Omnibus
GO	Gene ontology
GPL	GEO Platform
GSE	GEO series
GSH-Px	Glutathione peroxidase
H&E	Hematoxylin-eosin staining
HFHS	High fat high sucrose
HG	High glucose
HMGCS2	3-hydroxymethylglutaryl CoA synthetase 2
HW/TL	Heart weight to tibia length ratio
ID	Identification
IHC	Immunohistochemistry
IPGTT	Intraperitoneal glucose tolerance test
ITT	Insulin tolerance test
KEGG	Kyoto Encyclopedia of Genes and Genomes
LVEF	Left ventricular ejection fraction
LVFS	Left ventricular fractional shortening
MCODE	Molecular complex detection
MDA	Malondialdehyde
MF	Molecular Function
MFN1	Mitofusin 1
mtDNA	Mitochondrial DNA
NG	Normal glucose
nDNA	Nuclear DNA
OPA1	Optic atrophy 1
OXCT1	3-oxoacid CoA-transferase1
PBS	Phosphate buffered saline
PMID	PubMed identification
PPAR	Peroxisome proliferator-activated receptor
PPI	Protein-protein interaction
ROS	Reactive oxygen species
SD	Standard deviation
SGLT2	Sodium-glucose cotransporter 2
SOD	Superoxide dismutase
STRING	Search tool for the retrieval of interacting genes/proteins
STZ	Streptozotocin
T2D	Type 2 diabetes
TUNEL	Terminal deoxynucleotidyl transferase-mediated dUTP nick-end labeling
VEH	Vehicle
WGA	Wheat germ thrombin

3-hydroxybutyrate dehydrogenase (BDH1) expression level is associated with high-fat diet-induced type 2 diabetes [13]. 3-oxoacid CoA-transferase1 (OXCT1) is a rate-limiting ketolysis enzyme. In OXCT1 knockout mice, left ventricular volume increased, ejection fraction decreased, and mitochondrial ultrastructure was disturbed [14]. Those suggested that decreased ketone body oxidation may be a biological marker and therapeutic target for DCM. However, the specific mechanism of ketone metabolism in DCM remains unclear.

DCM is one of the leading causes of death in people with diabetes, and there is still a lack of effective treatments. Sodium-glucose cotransporter 2 (SGLT2) inhibitors entered the public eye as an oral drug for the treatment of T2DM. Multiple cardiovascular outcome trials have demonstrated that SGLT2 inhibitors have a proven cardiovascular benefit. Empagliflozin (Emp) was the first SGLT2 inhibitors drug to complete CVOTs [15]. Recently a series of large clinical trials, including the Dapagliflozin and Prevention of Adverse Outcomes in Heart Failure (DAPA-HF), the Empagliflozin Outcome Trial in Patients with Chronic Heart Failure and a Reduced Ejection Fraction (EMPEROR-Reduced) and the Empagliflozin Outcome Trial in Patients with Chronic Heart Failure with Preserved Ejection Fraction (EMPEROR-Preserved), have shown that SGLT2 inhibitors (SGLT2i) significantly reduce the risk of cardiovascular death in heart failure patients with or without diabetes [16–18]. Moreover, the degree of benefit was independent of left ventricular ejection fraction, which further confirmed that SGLT2 inhibits the cardioprotective effect independent of hypoglycemic mechanism, and pushes its cardiovascular benefit to non-diabetic heart failure population. Several mechanisms of beneficial cardiovascular effects of SGLT2 inhibitors have been hypothesized, such as attenuation of glucose toxicity, improvement of cardiac load conditions, amelioration of oxidative stress and improvement of cardiometabolism by increasing ketone bodies [19,20]. Among others, it has been shown that Emp inhibits oxidative stress and myocardial fibrosis by activating Nrf2/ARE signaling [21]. SGLT2i induces mild ketosis, suggesting a possible mechanism of action for its beneficial effect on heart failure in diabetic patients. Recent studies have shown that ketone bodies increase during SGLT2is treatment, which can reduce mortality and heart failure hospitalization in patients with the heart failure with preserved ejection fraction [22,23]. However, the role of ketone body metabolism and oxidative stress in the absence of heart failure in early DCM remains unclear. In addition, the regulation of Emp on DCM ketone metabolism is still lacking.

Therefore, in order to explore these issues, this study intends to explore the effects of Emp on myocardial ketone metabolism and oxidative stress in diabetic db/db mice based on the multiple Gene Expression Omnibus (GEO) database and the entry point of myocardial ketone metabolism of DCM. It provides theoretical basis for early diagnosis and treatment of DCM and prevention of heart failure.

2. Material and methods

2.1. Data preparation

We searched and downloaded mRNA expression data of DCM from the GEO (https://www.ncbi.nlm.nih.gov/geo/) using the keywords "diabetic cardiomyopathy" and "diabetic heart". The GSE215979, GSE161931, GSE145294, GSE161052, GSE173384, GSE123975, GSE161827, GSE210612 and GSE5606 were selected and downloaded for DEG analysis. All of the above raw data can be freely downloaded from the GEO database. These datasets met the following criteria: (1) the species was *Mus musculus* and Ratus norvegicus (GSE5606 only); (2) diabetic heart tissue and control tissue samples; (3) samples were replicated at least two times in the experiment. The corresponding platform annotation files from GEO series (GSE) were shown in Table 1.

2.2. Identification of differentially expressed genes

The "Limma", "DESeq2" and "RobustRankAggreg" package were used to identify differential expression genes (DEGs) between the DCM and the control group. The cutoff criteria were set as Log 2FC (fold change) > 1 and adjusted $P < 0.05$. We build the deg heatmap using the "Pheatmap" package and use the "ggplot2″ package to map the DEGs volcano. RobustRankAggreg method was used to integrate and analyze nine datasets GSE215979, GSE161931, GSE145294, GSE161052, GSE173384, GSE123975, GSE161827, GSE210612 and GSE5606, and the common DEGs was obtained. The list of upregulated and downregulated genes in each dataset was sorted by log2FC. The list of all genes was then integrated through the RobustRankAggreg package.

2.3. Animals models

All 8-week-old male diabetic db/db (BKs Cg-m +/+ Leprdb/J, a genetic mouse with spontaneous T2DM) and non-diabetic heterozygous db/m mice (n = 10 for each group) with body mass of 20–22 g (Si Pei Fu, China) were fed standard diet freely in SPF-grade animal house at room temperature (22 ± 2) °C, light/dark cycle for 12 h. They were divided into db/m, db/db and db/db + Emp groups, in which the db/db + Emp group was treated with drinking water containing Emp (10 mg/kg/day) for 8 weeks, body weight was measured after 2 months of treatment, and blood samples of each group were collected. Mice in each group were intraperitoneally injected with tribromoethanol (Avitine; 50 mg/kg) were sacrificed, the heart was removed, blood was taken for serum separation, and β-hydroxybutyrate (β-OHB) (Mlbio, China) and acetoacetate (AcAc) (Mlbio, China) levels were monitored. This study was approved by Experimental Animal Ethics Committee of Zhanjiang Central People's Hospital (ZJDY2023-53).

Table 1
GSE datasets used in this study.

Study Set	GEO Accession	Platform ID	Abbreviation (Number of Sample)	PMID
1	GSE215979	GPL24247 Illumina NovaSeq 6000	Ctrl Vs DM (6)	36706988
2	GSE161931	GPL24247 Illumina NovaSeq 6000	BKs Vs db/db (10)	35242109
3	GSE145294	GPL19057 Illumina NextSeq 500	CTR Vs T2D (4)	33303689
4	GSE161052	GPL21273 HiSeq X Ten	CK Vs DCM (6)	35173678
5	GSE173384	GPL24247 Illumina NovaSeq 6000	db/+ Vs db/db (10)	34368154
6	GSE161827	GPL19057 Illumina NextSeq 500	CD Vs HFHS (8)	34169737
7	GSE123975	GPL10787 Agilent-028005 SurePrint G3 Mouse GE 8 × 60 K Microarray	CON_VEH Vs CON_STZ (12)	32366681
8	GSE210612	GPL21810 Agilent-074809 SurePrint G3 Mouse GE v2 8 × 60 K Microarray	Control Vs Diabetic (6)	36078109
9	GSE5606	GPL1355 Affymetrix Rat Genome 230 2.0 Array	Normal Vs Diabetic (14)	17062650

2.4. Echocardiography and histological analysis

Transthoracic echocardiography was performed at 8, 12, and 16 weeks to assess cardiac structure and function. Echocardiographic parameters were measured and averaged over 3 consecutive cardiac cycles. Left ventricular end-systolic volume and left ventricular ejection fraction were measured by M-mode echocardiography. Based on in vivo echocardiographic studies of heart function, the hearts of each group were collected, weighed and the ratio to tibial length was calculated. Major organs such as the heart are fixed with a 10 % formalin buffer, embedded in paraffin, and cut into 5 μm thick sections. Hematoxylin-eosin staining (H&E), Masson staining, Wheat germ thrombin (WGA) staining, and Oil red O staining were used to observe the changes of myocardial pathology.

2.5. Fasting and random blood glucose levels and glucose tolerance tests

Fasting and random blood glucose levels were investigated at 8, 12, and 16 weeks. 16-week-old mice were subjected to insulin tolerance test (ITT) (0.5 U/kg) (n = 6) and intraperitoneal glucose tolerance test (IPGTT) (1 mg/g), respectively, and the area under the curve (AUC) was calculated.

2.6. TEM was used to detect the ultrastructural changes of myocardial tissue

The tissues were washed in phosphate buffered saline (PBS) and fixed in 2.5 % glutaraldehyde, then fixed with 1 % osmium tetroxide buffer, dehydrated with graded ethanol series and embedded in 812 resin. Ultrathin sections were stained with uranyl acetate water and lead citrate. The image was taken at JEM-100CX-II TEM (Joel, Japan) at 80 kV.

2.7. Culture and treatment of cardiomyocytes

To simulate the pathological environment of diabetes, H9C2 cardiomyocytes (ATCC) were subjected to normal glucose (5.5 mmol/L, NG) or high glucose (33 mmol/L, HG) conditions for 48 h. To test the potential therapeutic effect of Emp on H9C2 cardiomyocytes, HG medium was supplemented with 5 μM Emp (Selleckchem, USA).

2.8. Apoptosis assay

Apoptosis in cardiac tissues was analyzed using the terminal deoxynucleotidyl transferase-mediated dUTP nick-end labeling (TUNEL) assay kit (C1090, Beyotime, China), using the procedure according to the manufacturer's instructions. The apoptosis rate of H9C2 cells was analyzed by flow cytometry using the annexin V-APC/PI apoptosis kit (E-CK-A217, Elabscience, China) following the manufacturer's instructions.

2.9. Mitochondrial isolation

Cardiomyocytes were isolated from mouse heart tissue by centrifugal precipitation. The cells were centrifuged at 1200 r/min for 5 min, the

supernatant was discarded, and the cell precipitate was resuspended with 5 % FCS/DMEM medium and incubated in an incubator; after 90 min of cell apposition, the suspension of unapproximated cardiomyocytes was aspirated as described previously [24]. The mitochondria were isolated from cardiomyocytes using a mitochondrial isolation kit (C3601, Beyotime, China). The total mitochondrial protein concentration was determined by BCA protein assay kit (P0010S, Beyotime, China).

2.10. Enzyme activities of HMGCS2, OXCT1and BDH1

Mouse hearts were collected and immediately assayed for enzyme activity. HMGCS2, OXCT1 and BDH1 enzyme activities were measured as previously described [13,25,26]. Enzyme activities were expressed as mmol/min/g protein.

2.11. β-OHB and AcAc concentrations

β-OHB levels in mouse frozen heart tissue, serum and urine were determined using a β-hydroxybutyric acid colourimetric kit (JL-T1392, JianglaiBio, China) according to the manufacturer's instructions. AcAc levels in myocardial tissue and serum were determined using a mouse acetoacetate enzyme-linked immunosorbent assay (ELISA) kit (2M-KMLJM220724 m, Camilo, China).

2.12. Mitochondrial DNA (mtDNA) to nuclear DNA (nDNA) ratio

Total DNA from mouse hearts was extracted using the DNeasy Blood and Tissue Kit (69504, QIAGEN, Germany). mtDNA and nuclear DNA copy numbers were quantified by real-time qPCR of cytochrome *b* and β-actin, respectively, as described previously [27].

2.13. Mitochondrial electron transport chain (ETC) analysis

An ELISA microplate assay kit (M150924-8, Mreda, China) was used to measure mitochondrial respiratory chain complex activity according to the manufacturer's instructions. Results are expressed as relative activity (specific respiratory chain complex activity/citrate synthase activity).

2.14. Cardiomyocyte mitochondrial reactive oxygen species (ROS), ATP and oxidative markers assessment

MitoSOX Red staining (M36008, Invitrogen, USA) was used to assess mitochondrial ROS levels in cardiac tissues. Mitochondrial ROS was detected in H9C2 cells using a ROS assay kit (S0033, Beyotime, China), and then detected using flow cytometry according to the protocol provided by the manufacturer. ATP concentration in the cardiomyocytes was measured using an ATP assay kit (S0026, Beyotime, China), following the manufacturer's instructions. The results of each assay were normalized by protein concentration as described previously [28]. The results were shown as mmol/mg protein. The levels and activities of superoxide dismutase (SOD), glutathione peroxidase (GSH-Px), Catalase (CAT) and malondialdehyde (MDA) were measured according to the ELISA kit instructions to further assess the level of oxidative stress (2 R-KMLJr30259, 2M-KMLJM220779 m, 2M-KMLJM220658 m, 2M-KMLJM219464 m, Camilo, China). The levels of 4-hydroxy-2-nonenal (4-HNE), 3-nitrotyrosine (3-NT), and protein carbonyl in myocardial tissues were determined using an ELISA assay kit (

CSB-E13411-13 m, Cusabio, China), and were expressed in nmol/mg protein as measured according to the manufacturer's protocol.

2.15. Immunofluorescence staining

Myocardium sections or cell suspensions were inoculated in petri dishes, fixed with pre-cooled 4 % paraformaldehyde, and rinsed with PBS 3 times for 5 min each time. Block serum (5%FBS+0.01 % Triton X-100 dissolved in PBS) was added and incubated at 37 °C for 60 min. After sealing, diluted Nrf2 (1:50, Abcam) was added to a wet box at 4 °C overnight, and rinsed with PBS 3 times for 5 min each time. Red fluorescent secondary antibody (1:200) was added away from light, incubated at 37 °C for 30 min, and rinsed 3 times with PBS for 5 min each time. The anti-fluorescence quenching sealing tablets containing 4′, 6-diamidino-2-phenylindole (DAPI) were observed under fluorescence microscope.

2.16. qRT-PCR

Total RNA was extracted by TRIzol method. The purity and concentration of RNA were determined, and then reverse-transcribed into cDNA, and qRT-PCR was performed by StepOne Plus real-time fluorescence quantitative PCR. The primers were synthesized by GenePharma (Table S1). Data were processed using $2^{-\Delta\Delta CT}$ method.

2.17. Western blot

It was used to detect key enzymes of target ketone bodies, mitochondrial markers, apoptosis and main regulatory factors of antioxidant stress protein levels. Type-specific antibodies were shown in Table S2. The protein was extracted by adding cell lysate and protease inhibitor. Protein samples were taken for electrophoresis. After electrophoresis, the film was transferred, 5 % skim milk powder was enclosed at room temperature for 1 h, then antigen and antibody reaction were performed, and the target bands of the images were exposed in a dark room according to the instructions of the enhanced chemiluminescence (ECL) luminescence kit (P0018 M, Beyotime, China). Finally, the Image J software was used for gray analysis.

2.18. Immunohistochemistry (IHC)

The expression levels of key ketone metabolizing enzyme protein in the heart of each group were detected by IHC. Paraffin sections of mouse hearts were routinely dewaxed to water, antigen repair, PBS washing, added to the configured primary antibody (Table S2), and overnight on a rocking bed at 4 °C; After repeated washing with PBS, adding secondary antibody, diaminobenzidine (DAB) color development, gradient dehydration with ethanol, xylene transparent, neutral resin seal, observation under microscope.

2.19. Statistical analysis

Statistical analysis was performed using GraphPad Prism 9.0 and R software. Experimental data are expressed as mean ± standard deviation (SD). Comparisons among multiple groups were made by a one-way analysis of variance (ANOVA), followed by a Tukey post hoc analysis to determine statistical significance. Values of $P < 0.05$ was considered to be statistically significant.

3. Results

3.1. Identification of DEGs in diebetic hearts

By utilizing the high-throughput Gene Expression GEO database combined analysis of GSE215979, GSE161931, GSE145294, GSE161052, GSE173384, GSE123975, GSE161827, GSE210612 and GSE5606. The 9 DCM expression datasets, totaling 38 pairs of samples, are shown in Fig. 1A for a simple flow chart. R-package RobustRankAggreg was used for final expression analysis of 9 different chips or high-throughput sequencing, and the adjusted *P* value < 0.05 was the standard. 259 DEGs were obtained, among which 226 genes were up-regulated and 33 mRNA were down-regulated. the heatmap for the top 20 DEGs is displayed in Fig. 1B, in addition, Heat maps show the top

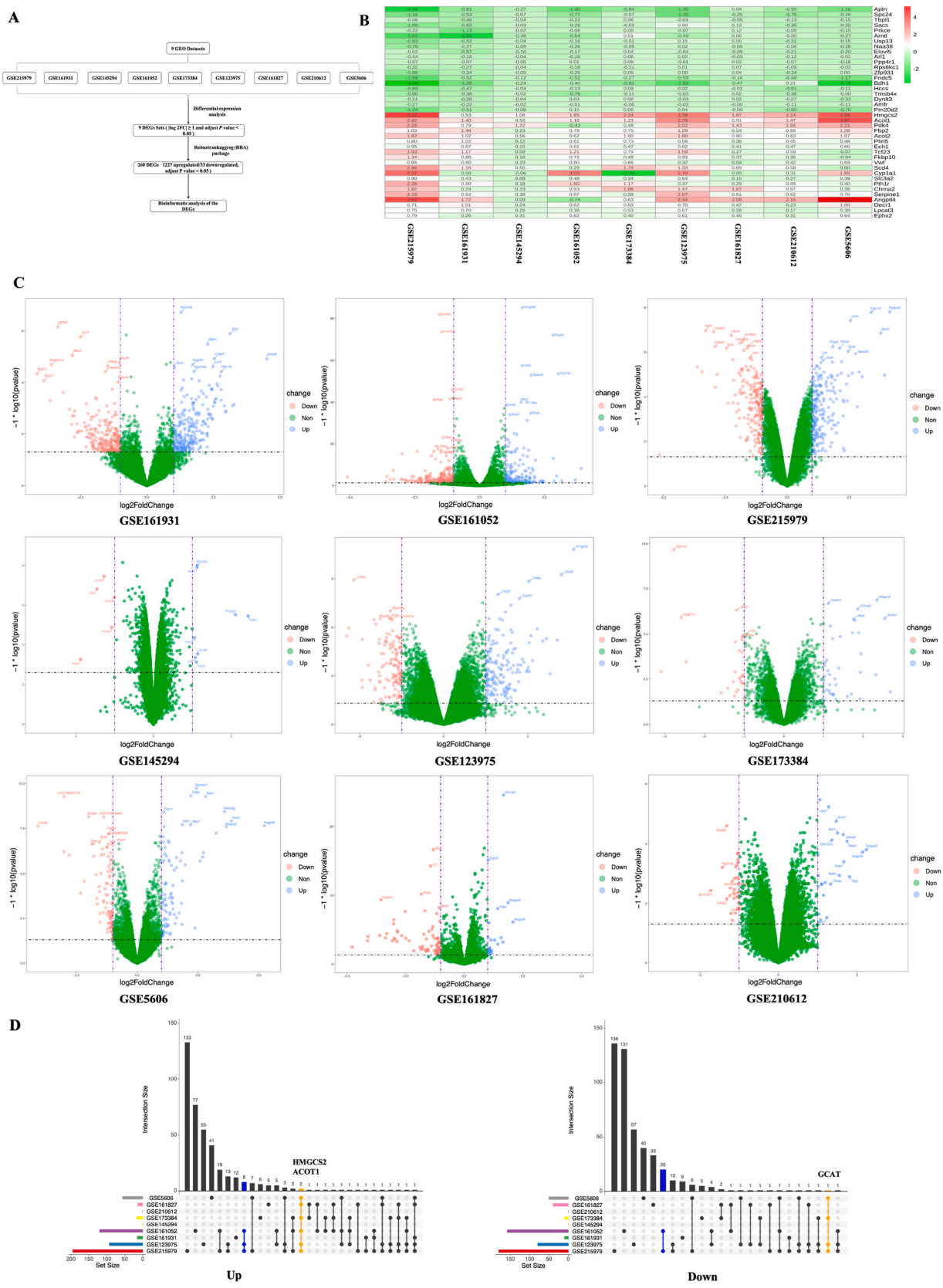

Fig. 1. Identification of DEGs and overlapping DEGs in the Diabetic or non- Diabetic heart. (A) Experimental flowchart. Gene expression profiles from the GEO public dataset were analyzed to identify DEGs in cardiac tissue. (B) log2FC heat maps representing the image data of each microarray. Note: The horizontal coordinate is GEO ID, and the vertical coordinate is the name of the gene. Blue indicates log2FC > 1, red indicates log2FC < 1 (except GSE145294). (C) Volcano map of differentially expressed RNA in each gene chip. (D) UpSetR plot with 9 data sets overlapping homologous DEGs. (For interpretation of the references to colour in this figure legend, the reader is referred to the Web version of this article.)

80 DEGs using the R package RobustRankAggreg in Fig. S1. Volcanoes were mapped using ggplot2 to show up-regulated and down-regulated genes in 9 datasets respectively (Fig. 1C). Using the adjusted P value < 0.05 and Log2FC ≥ 1 as the criteria, no differential genes were obtained in the GSE145294 and GSE210612 datasets, while 404 up-regulated genes and 464 down-regulated genes were obtained in the other 7 datasets. The results were visualized using UpSetR package (Fig. 1D). Among the up-regulated genes, "GSE215979″, "GSE123975″, "GSE161052″, "GSE161827″, "GSE173384″ and "GSE5606″ were intersected to obtain HMGCS2 and acyl-CoA thioesterase 1 (ACOT1) overlapping genes. Among the down-regulated genes, "GSE215979″, "GSE123975″, "GSE173384″ and "GSE5606″ share a GCAT overlapping gene. The heat map shows that the top 10 differential genes up-regulated and down-regulated are shown in Fig. 2A, and the summary heat map of DEGs is shown in Fig. 2B.

3.2. Significant enrichment analysis in DCM

Integration of transcriptional analysis to identify 9 sets of gene expression profiles downloaded from the differential expression gene bank and gene ontology analysis (GO annotation) showed that these differential genes were mainly involved in metabolic processes and transport processes. Database for Annotation, Visualization and Integrated Discovery (DAVID) software was used to perform GO enrichment analysis on Upregulated differentially expressed proteins, and the results showed that 221 out of 226 upregulated differentially expressed proteins were successfully annotated to 996 GO functional items (Fig. 3A, upper left). Biological process (BP) accounted for 921 functional items, the most significant of which were metabolic processes and transport processes, including fatty acid metabolism, small molecule catabolism, cellular ketone metabolic process, regulation of muscle cell apoptosis, ribonucleotide metabolism and regeneration. Cellular Component (CC) accounted for 16 functional items, indicating that differential proteins were mainly distributed in cytoplasm, cell membrane and intracellular. Molecular Function (MF) accounted for 59 functional items, indicating that differential proteins mainly have binding activities, cleavage activities and transport activities, including transcription co-regulatory factor binding, ligand-activated transcription factor activity and core promoter sequence-specific DNA binding.

We performed the Kyoto Encyclopedia of Genes and Genomes (KEGG) pathway analysis on DEGs and found that 30 up-regulated pathways were significantly enriched ($P < 0.05$, upper right of Fig. 3A). Circos chart shows key up-regulated and down-regulated DEGS for critical GO enrichment (Fig. 3B upper right). Notably, HMGCS2 is associated with acetyl-CoA metabolic processing and cellular carbohydrate processing. Further, in order to understand the key molecular mechanism of DCM, we conducted GSEA analysis based on differential gene expression, and the results showed that differential genes were mainly involved in Hippo signaling pathway (NES = 1.85), Peroxisome proliferator-activated receptor (PPAR) signaling pathway (NES = 2.45) and unsaturated fatty acid biosynthesis (NES = 2.06) (Fig. 3C). The expression analysis of PPAR signaling pathway molecules was finally achieved by R package RobustRankAggreg. The calibration P value $<$ 0.05 was the standard, and HMGCS2 showed similar high expression behavior in different GEO data sets (Fig. 3D).

3.3. Construct protein-protein interaction (PPI) networks

Input the obtained 260 DEGs into the search tool for the retrieval of interacting genes/proteins (STRING) database (Version: 11.5) and a protein-protein interaction (PPI) network was constructed, obtaining a total of 259 nodes and 750 connections, as shown in Fig. 4A. In order to further explore the possible protein interaction modules with core significance in PPI network, the molecular complex detection (MCODE) plug-in in Cytoscape software was utilized for module mining and analysis. The results showed that the protein module with the highest score (score = 14.444) contained 19 nodes and 130 connections as shown in Fig. 4B. In the MCODE cluster, Acaa2, Dhrs4, Hsd17b4, Cpt1a, Acadl, Etfdh, Decr1, Hsdl2, Acsl1, Acot1, Eci2, Ech1, Acox1, Acadvl, Hadha, Acot2, Acot3, and Ephx2 are interactors of HMGCS2 (Fig. 4B). More importantly, the analysis based on the constructed protein interaction network found that HMGCS2 was in the core position of the interaction network. In addition, GO enrichment analysis showed that the biological processes mainly focused on 27 BP entries such as fatty acid metabolic process, oxidation-reduction process, acyl-CoA metabolic process and regulation of fatty acid oxidation. MF mainly focused on 20 molecular function entries such as catalytic activity and oxidoreductase activity, CC mainly focused on 10 entries such as mitochondrion and peroxisome (Fig. 4C). KEGG pathway enrichment analysis included peroxisome, metabolic pathways and PPAR signaling pathway, etc. (Fig. 4D). It is suggested that HMGCS2 has important research value in the occurrence and development of DCM.

3.4. Expression of key enzymes of ketone body metabolism in myocardium of DCM

In order to clarify the role of key enzymes of ketone body metabolism in myocardial tissue in the pathogenesis of DCM, we observed the expression levels of HMGCS2, BDH1 and OXCT1 in db/db myocardial tissue at weeks 8, 12 and 16, respectively, HMGCS2 enzyme activity was increased in the DCM heart, while ketolysis enzymes BDH1 and OXCT1 expression were inhibited compared with db/m (Fig. 5A–C), and myocardial immunohistochemistry at weeks 8 and 16 showed the same results (Fig. 5D).

3.5. Emp alleviates heart dysfunction in db/db mice

Cumulative cardiovascular trials have shown that SGLT2 inhibitors reduce cardiovascular risk in the diabetic population, but the exact mechanisms behind such clinical benefits remain to be elucidated. db/db mice exhibited significantly higher fasting, random glucose levels, and heavier body weight compared to db/m mice (Fig. 6B). After 8 weeks of treatment, the fasting and random blood glucose levels and body weight of the db/db + Emp group were significantly decreased (Fig. 6B), and there was no difference in organ H&E staining among the groups (Fig. S2). To better understand the role of Emp, we examined IPGTT and ITT. As shown in Fig. 6C, after 8 weeks of Emp (10 mg/kg/d) treatment and 120 min after glucose administration, glucose tolerance improved significantly compared to untreated db/db mice. Similarly, db/db + Emp effectively controlled blood glucose levels 90 min after insulin administration, indicating gradual improvement in insulin resistance (Fig. 6D). In addition, echocardiographic analysis was performed to determine whether Emp treatment improved cardiac function in db/db mice (Fig. 6E and F). The results showed that compared with db/m mice, db/db mice had impaired cardiac function with lower left ventricular ejection fraction (LVEF) and left ventricular fractional shortening (LVFS) and higher left ventricular posterior wall thickness at end-systole (LVPWs) and end-diastole (LVPWd). In contrast, the db/db + Emp mice had significantly improved cardiac function, with higher LVEF and LVFS scores than the control db/db mice.

3.6. Emp improves histological abnormalities in db/db mice

After 8 weeks of treatment, the heart enlargement in the db/db + Emp group was significantly smaller than that in the db/db group (Fig. 7A), and the heart weight to tibia length ratio (HW/TL) was lower than that in the db/db group (Fig. 7B). Myocardial histological analysis was performed using H&E, WGA, Masson trichrome staining, oil red O staining, and TUNEL method (Fig. 7A). H&E and WGA showed that the db/db + Emp group reduced the left ventricular septal thickness and attenuated cardiomyocyte hypertrophy as compared to the db/db group (Fig. 7 A, C). Consistent with this, Masson staining showed that db/db +

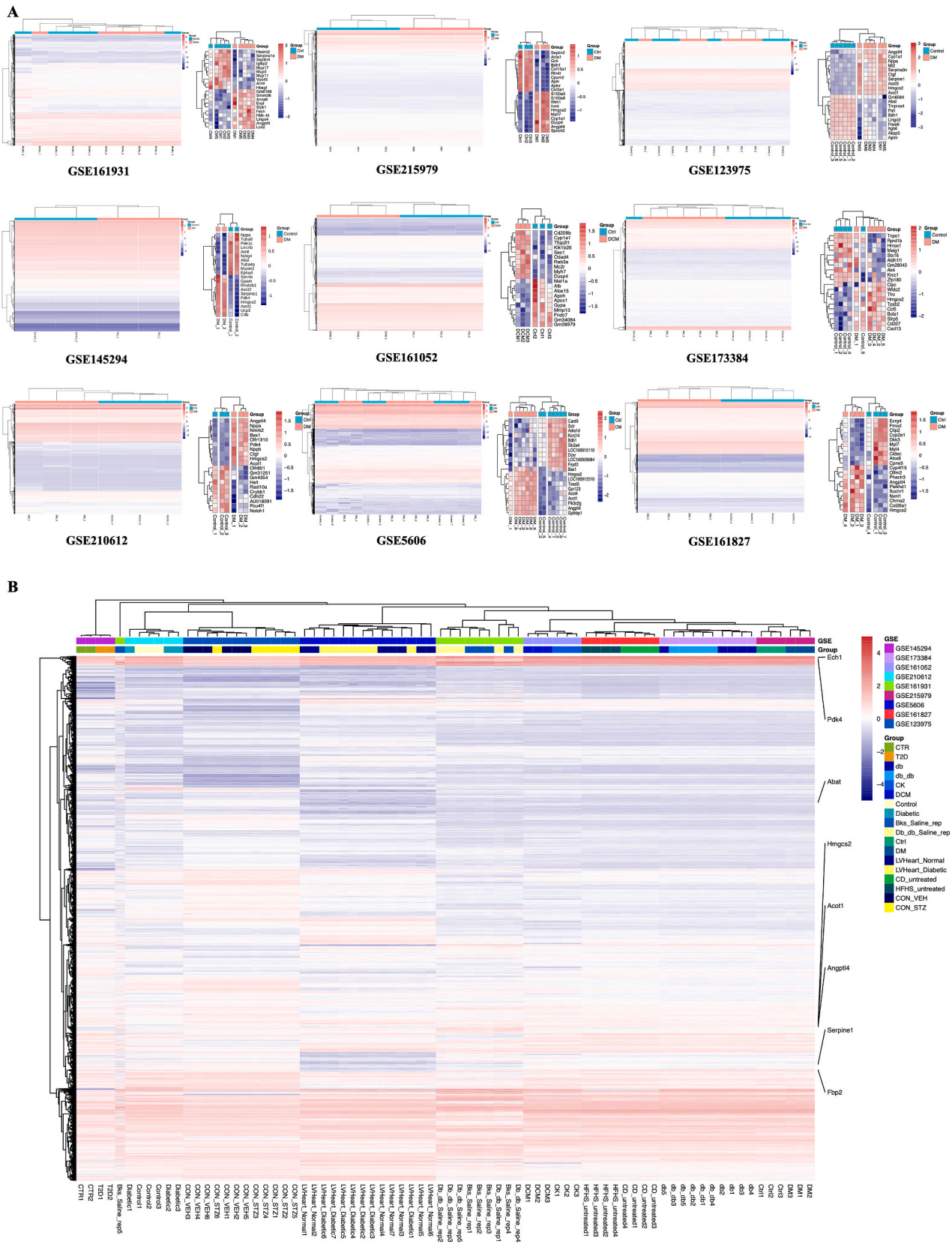

Fig. 2. Heat maps of 9 GSE datasets. (A) Representative image of the heat map, the one on the right shows the top 10 DEGs genes between DM and Control. (B) Differential gene expression heat maps were collected from 9 datasets. Gradients of red and blue represent high and low levels of expression. The GSEs, Groups, and key genes have been labeled in their respective locations. (For interpretation of the references to colour in this figure legend, the reader is referred to the Web version of this article.)

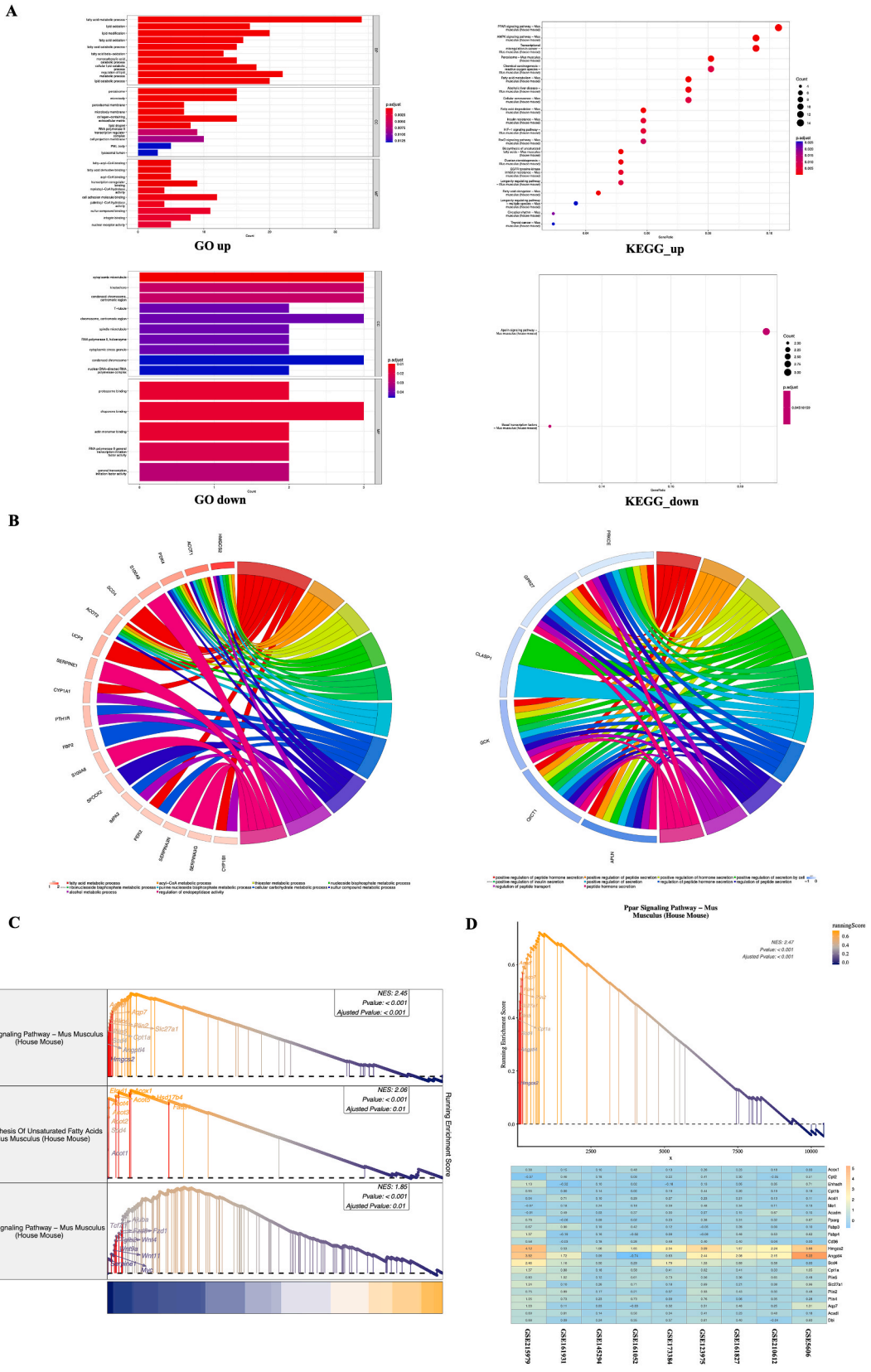

Fig. 3. Functional enrichment analysis in DCM. (A) Enrichment analysis of differentially expressed genes GO and KEGG. The figure shows the GO and KEGG analysis results of up-regulated and down-regulated mRNA respectively ($P < 0.05$). (B) Circos maps show up-regulated and down-regulated DEGs for critical GO enrichment. (C) DEGs gene set enrichment analysis (GSEA). (D) R package RobustRankAggreg finally realized the expression analysis of PPAR signaling pathway molecules (11 up-regulated and 11 down-regulated).

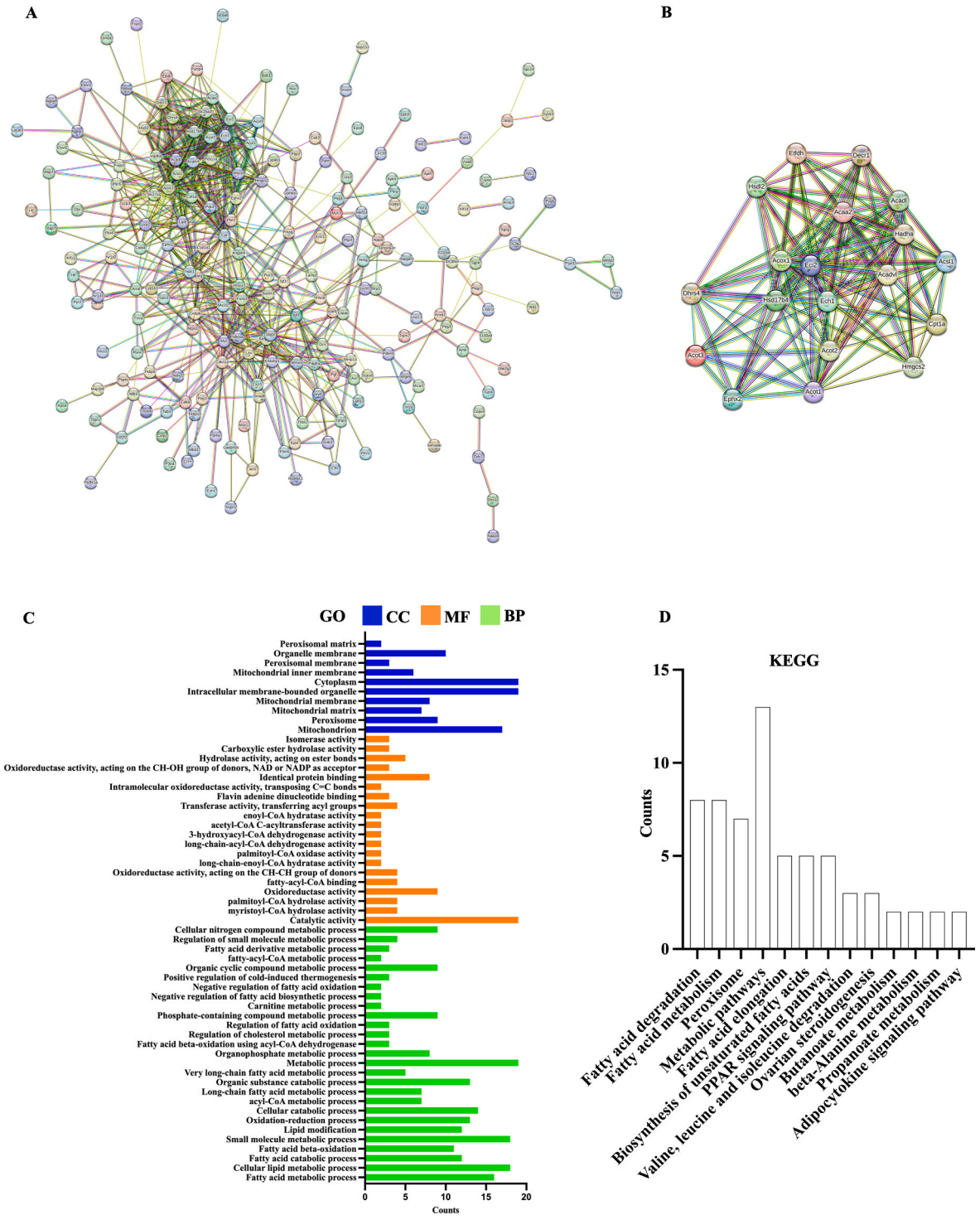

Fig. 4. Differential protein interaction network. (A) 259 DEGs interaction networks were constructed using STRING database, and (B) protein-protein interaction networks encoding proteins from 19 candidate genes. (C, D) GO and KEGG enrichment analysis of core genes.

Emp attenuated myocardial fibrosis in db/db. Oil red O staining showed less myocardial lipid accumulation in the db/db + Emp group compared with the db/db group, but the difference was not statistically significant. Finally, to further assess the level of apoptosis in cardiomyocytes, TUNEL staining was performed, and the percentage of TUNEL-positive nuclei was reduced in the db/db + Emp group. In addition, the hypertrophic gene ANP mRNA and protein levels were significantly reduced (Fig. 7 D). The results of the relative quantitative data are shown in the lower right Fig. 7E. Thus, Emp significantly ameliorated cardiac hypertrophy and dysfunction.

3.7. Emp promotes ketone body metabolism and ameliorates cardiac mitochondrial dysfunction in db/db mice

3.7.1. Emp promotes ketone body metabolism

To clarify the effect of Emp on myocardial ketone body metabolism, key synthetic and catabolic enzymes in the ketone body metabolic pathway were examined. We found that the expressions of ketolysis

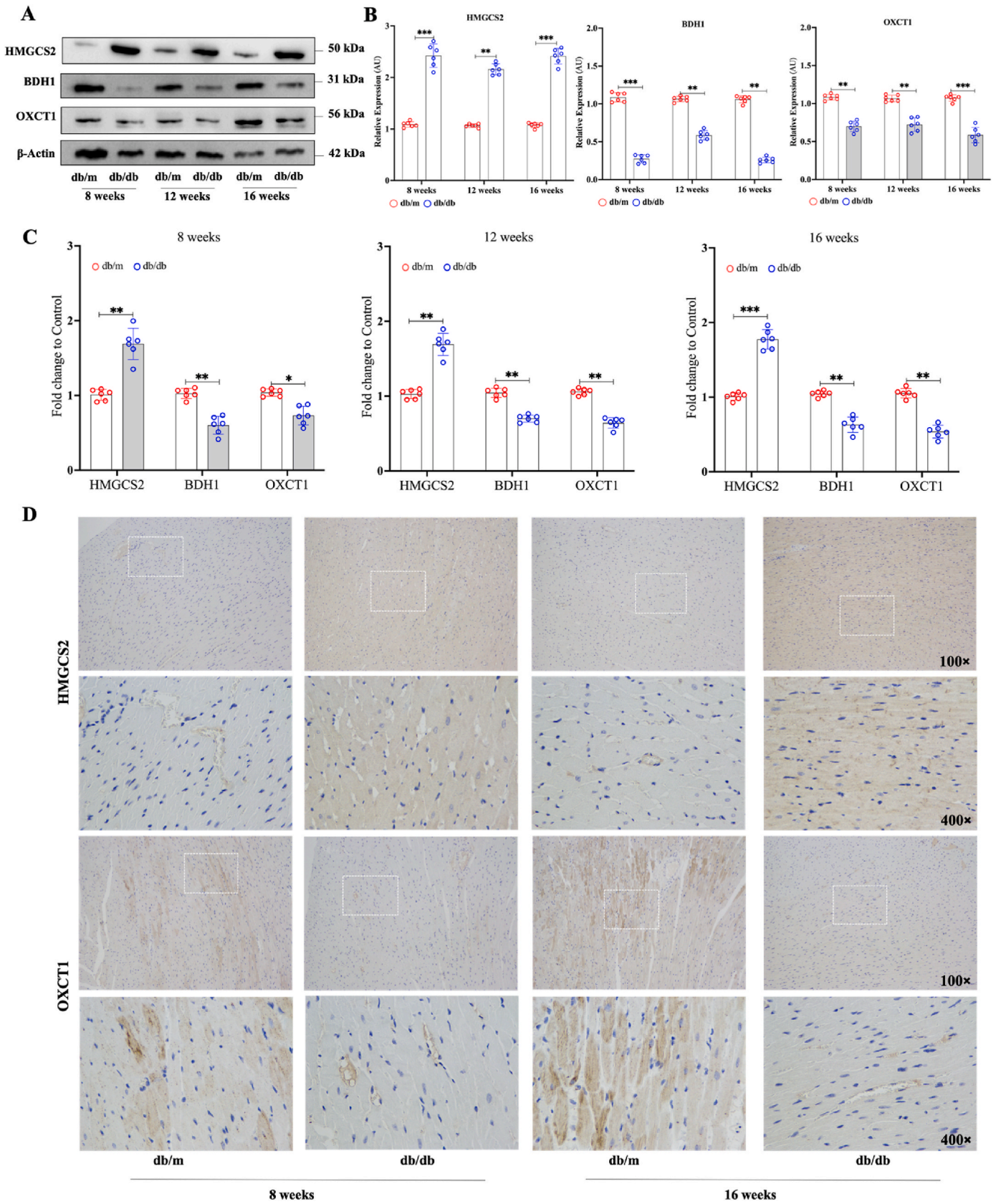

Fig. 5. Expression of key enzymes of ketone metabolism in myocardium of DCM. (A) The representative protein expressions of HMGCS2, BDH1 and OXCT1 in the myocardium of db/db and db/m groups were analyzed by Western Blot at weeks 8, 12 and 16, with β-actin as the loading control. (B) Density quantification of representative Western Blot, n = 6. (C) mRNA expression levels of HMGCS2, BDH1 and OXCT1 were confirmed by qRT-PCR. n = 6. (D) Immunohistochemical staining micrographs of HMGCS2, BDH1 and OXCT1 in db/db mouse myocardium (100 × and 400 ×). Data were mean ± SD; $^{*}P < 0.05$, $^{**}P < 0.01$, $^{***}P < 0.001$.

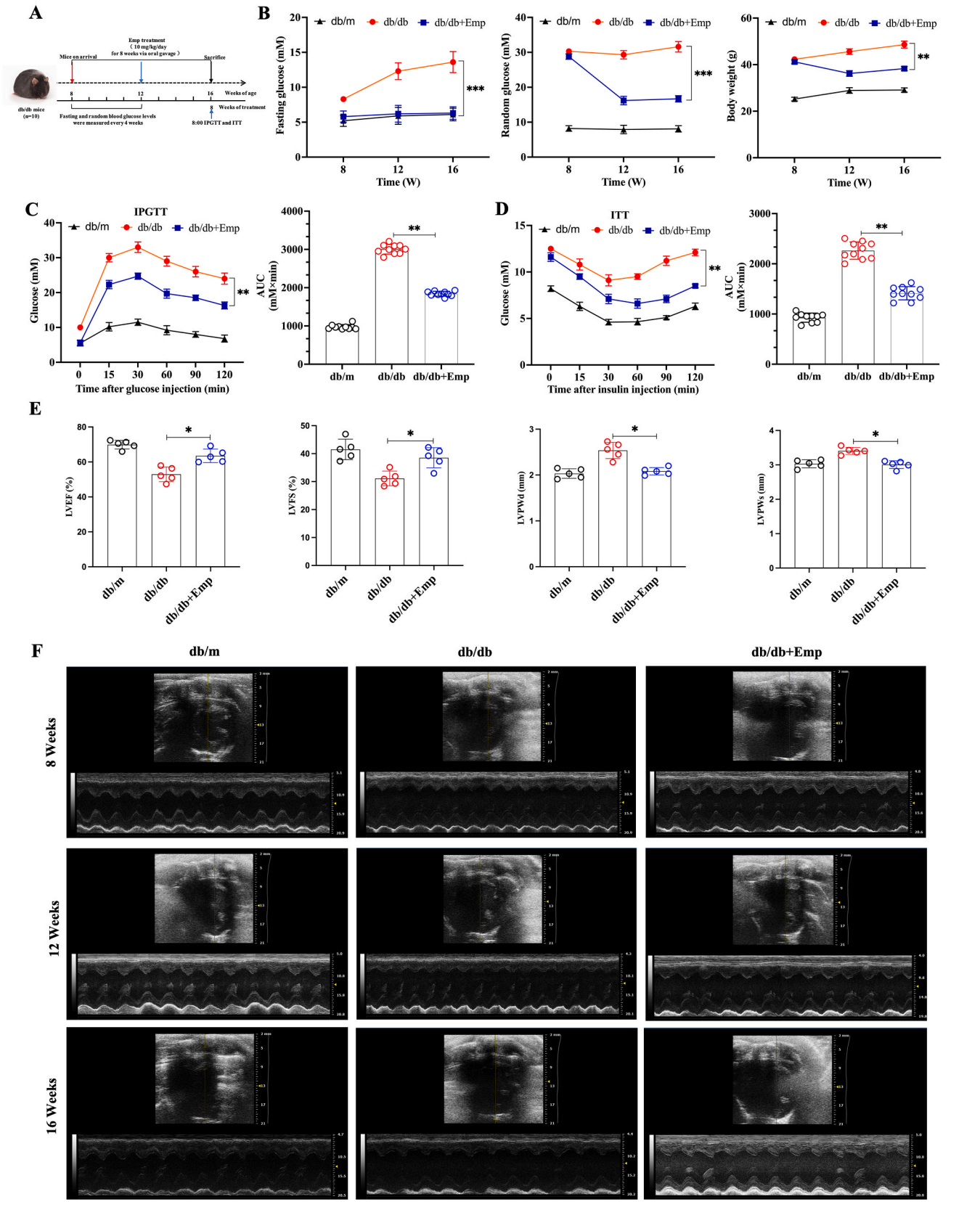

Fig. 6. Emp improves heart function in db/db mice. (A) Experimental flow chart. (B) Fasting, random blood glucose level and body weight changes were observed in different groups during the study period. (C) IPGTT and (D) ITT were analyzed after intraperitoneal injection of glucose (2 g/kg) and insulin (5 U/kg), respectively, on day 35 after fasting for 4 h. Blood glucose was measured from baseline (0) to 120 min. Results are expressed as mean ± SD (n = 10). (E) Values of LVEF, LVPWd and LVPWs in each group. n = 5. Data were expressed as mean ± SD, $^{*}P < 0.05$; $^{**}P < 0.01$, $^{***}P < 0.001$.

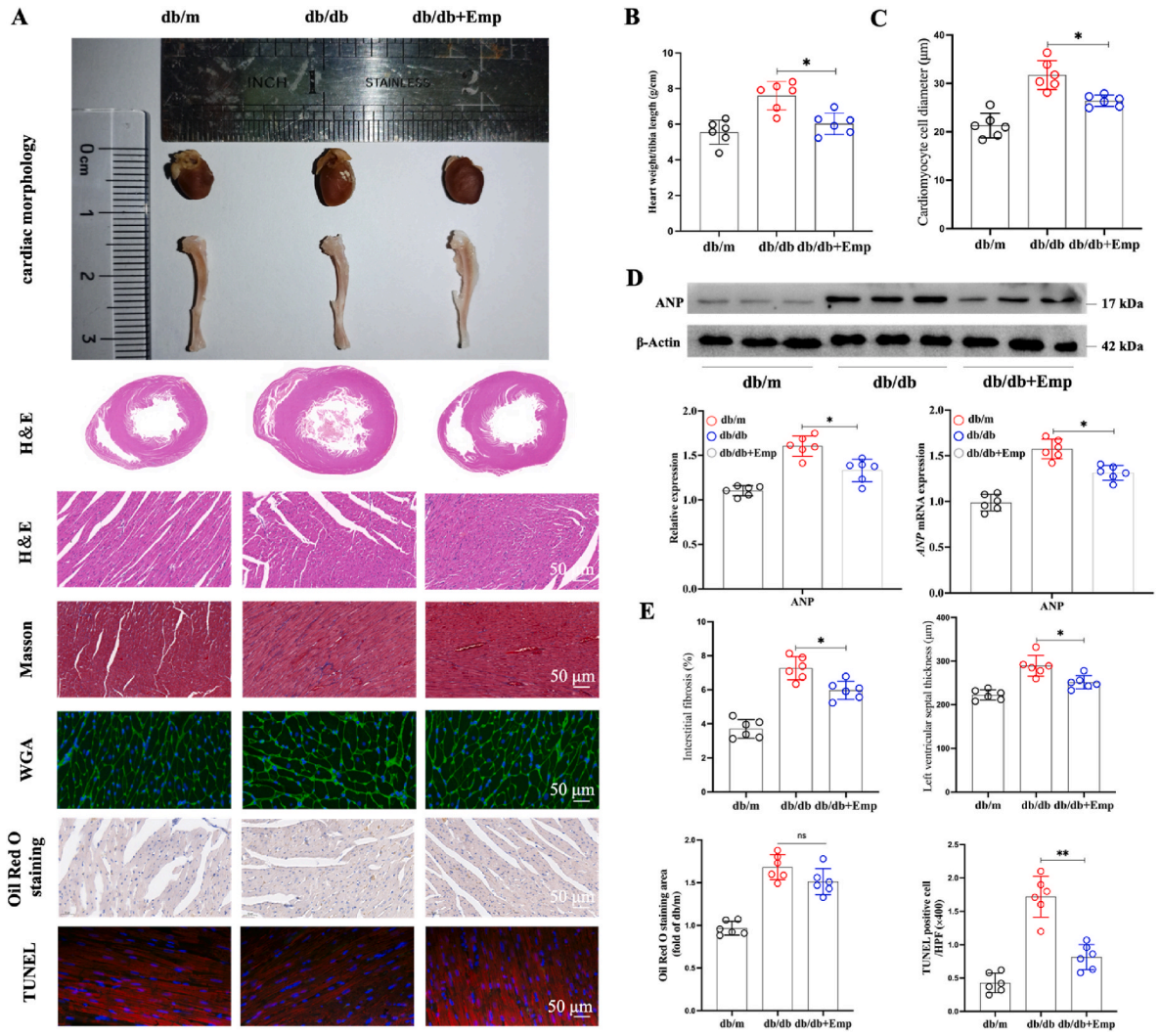

Fig. 7. Emp improves histological abnormalities in diabetic mice. (A) Cardiac morphology, H&E staining, Masson staining, WGA staining, oil red O staining and Tunel representative images. (B) The ratio of the weight of the heart to the length of the tibia, n = 6 in each group. (C) Emp decreased cardiomyocyte area. (D) mRNA and protein expression of ANP was measured by qRT-PCR and Western Blot. (E) Quantitative analysis of representative cross-section images by group. Data were expressed as mean ± SD, n = 6, $^{*}P < 0.05$; $^{**}P < 0.01$. (For interpretation of the references to colour in this figure legend, the reader is referred to the Web version of this article.)

enzymes BDH1 and OXCT1 in db/db group were significantly decreased, and the expression levels of BDH1 and OXCT1 were increased after Emp treatment. HMGCS2 expression was also increased in the DCM heart compared to the db/db group (Fig. 8A–C). In the db/db + Emp group, the activities of the ketone body synthase HMGCS2 and the ketone body catabolic enzymes BDH1 and OXCT1 were significantly elevated compared with the db/db group (Fig. 8D–F). Serum, myocardial tissue, and urinary levels of β-OHB were significantly elevated in EMPA-treated db/db mice compared with those in the db/db group, and AcAc levels were also significantly increased (Fig. 8G).

3.7.2. Emp ameliorates mitochondrial dysfunction in the heart of db/db mice

Mitochondria are the main site of ketone body metabolism, and ketone bodies serve as a good fuel for mitochondria to produce ATP and provide more energy for cells. Myocardial transmission electron microscopy analysis showed that the db/db group resulted in a large number of mitochondrial irregularities and structural distortions, whereas the db/db + Emp group ameliorated the structural distortions of mitochondria (Fig. 9A). This included reductions in mitochondrial area and bulk density after Emp treatment, as well as significant reductions in the total value density of damaged mitochondria in the db/db + Emp group compared to the db/db group (Fig. 9B and C). Cardiomyocytes in the db/db + Emp group contained more copies of mtDNA per nuclear genome compared with the db/db group (Fig. 9D). To determine the effect of EMP supplementation on cardiomyocyte energy, myocardial ATP levels were measured. As shown in Fig. 9E, ATP levels in the cardiac tissue of mice in the db/db + Emp group were higher than those in the db/db group. In addition, we investigated the expression of Mitofusin 1 (MFN1), Optic atrophy 1 (OPA1) and Dynamin-associated protein 1 (DRP1) in cardiac tissue related to mitochondrial dynamics. The results showed that compared with db/m group, the expression of mitochondrial fusion markers MFN1 and OPA1 was down-regulated, and the expression of mitochondrial fission marker DRP1 was up-regulated. After Emp treatment, the expression of mitochondrial division markers DRP1 was down-regulated, while the expression of MFN1 and OPA1 was up-regulated (Fig. 9F). We further assessed whether Emp affects db/db mitochondrial electron transport chain activity, and the activity of the complexes has been normalized with citrate synthase, which increased in the db/db + Emp group compared to the db/db group, with the exception of complex-II (Fig. 9G).

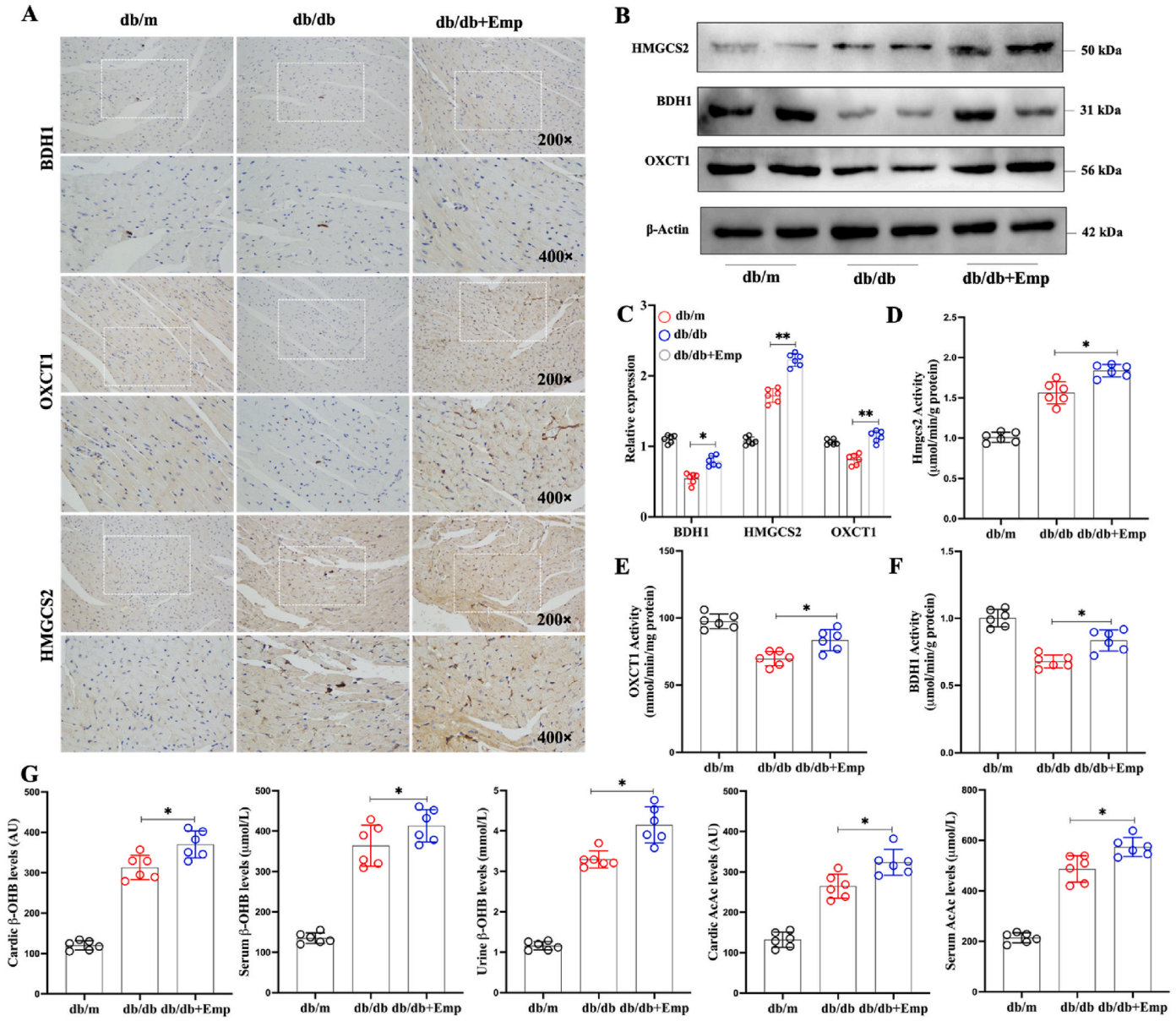

Fig. 8. Emp promotes ketone body metabolism in db/db mice. (A) Micrographs of immunohistochemical staining of myocardial tissues of HMGCS2, BDH1, and OXCT1 in mice in each group (200 × and 400 ×). (B) Western blot analysis of representative expression of HMGCS2, BDH1 and OXCT1 proteins in myocardial tissues of mice in the db/db and db/m groups, with β-actin as a loading control. (C) Densitometric quantification of representative Western blots, n = 6. (D–F) Activities of the ketone body synthase HMGCS2 and the ketone body catabolic enzymes BDH1 and OXCT1. (G) Levels of β-OHB and AcAc in serum, myocardial tissue and urine of mice in each group. The data were expressed as mean ± SD, n = 6. *$P < 0.05$, **$P < 0.01$.

3.8. Emp improves intracellular oxidative stress in cardiomyocytes of db/db mice

Mitochondrial ROS expression was increased in cardiac tissues of db/db mice compared with db/m mice, and MitoSOx-positive cells were reduced after Emp treatment (Fig. 10A). Consistent with these findings, the expression of SOD, GSH-Px, and CAT was also significantly increased in db/db mice compared with db/m mice, whereas MDA levels were significantly reduced, but these changes improved significantly after Emp treatment and SOD, GSH-Px and CAT enzyme activities were also elevated (Fig. 10B). The transcription factor Nrf2 is a major regulator of antioxidant and stress responses. Nuclear Nrf2 immunofluorescence was significantly higher in the Emp-treated group than in the untreated db/db mouse group, and in addition Emp treatment increased nuclear Nrf2 protein and mRNA levels (Fig. 10C). Finally, we measured the effects of Emp treatment on oxidative stress damage in cardiac tissue, and found that the levels of 3-NT, 4-HNE and protein carbonyl, markers of oxidative damage, accumulated to a high level in the hearts of db/db mice, whereas treatment with Emp significantly attenuated these effects. In summary, Emp attenuated diabetes-induced oxidative stress in the heart (Fig. 10D).

3.9. Emp promotes the expression of HG-induced ketolysis enzymes in cardiomyocytes and inhibits oxidative stress and apoptosis

To assess the intrinsic activity of Emp on ketone body metabolism in DM cardiomyocytes, we used cultured H9C2 cells exposed to HG stimulation. Next, we examined the expression levels of key enzymes of ketone body metabolism. The results showed that HG induced a decrease in the expression of the ketone body metabolism genes BDH1 and OXCT1, whereas no significant changes were seen in the ketogenic key enzyme HMGCS2, and the treatment with Emp increased the protein

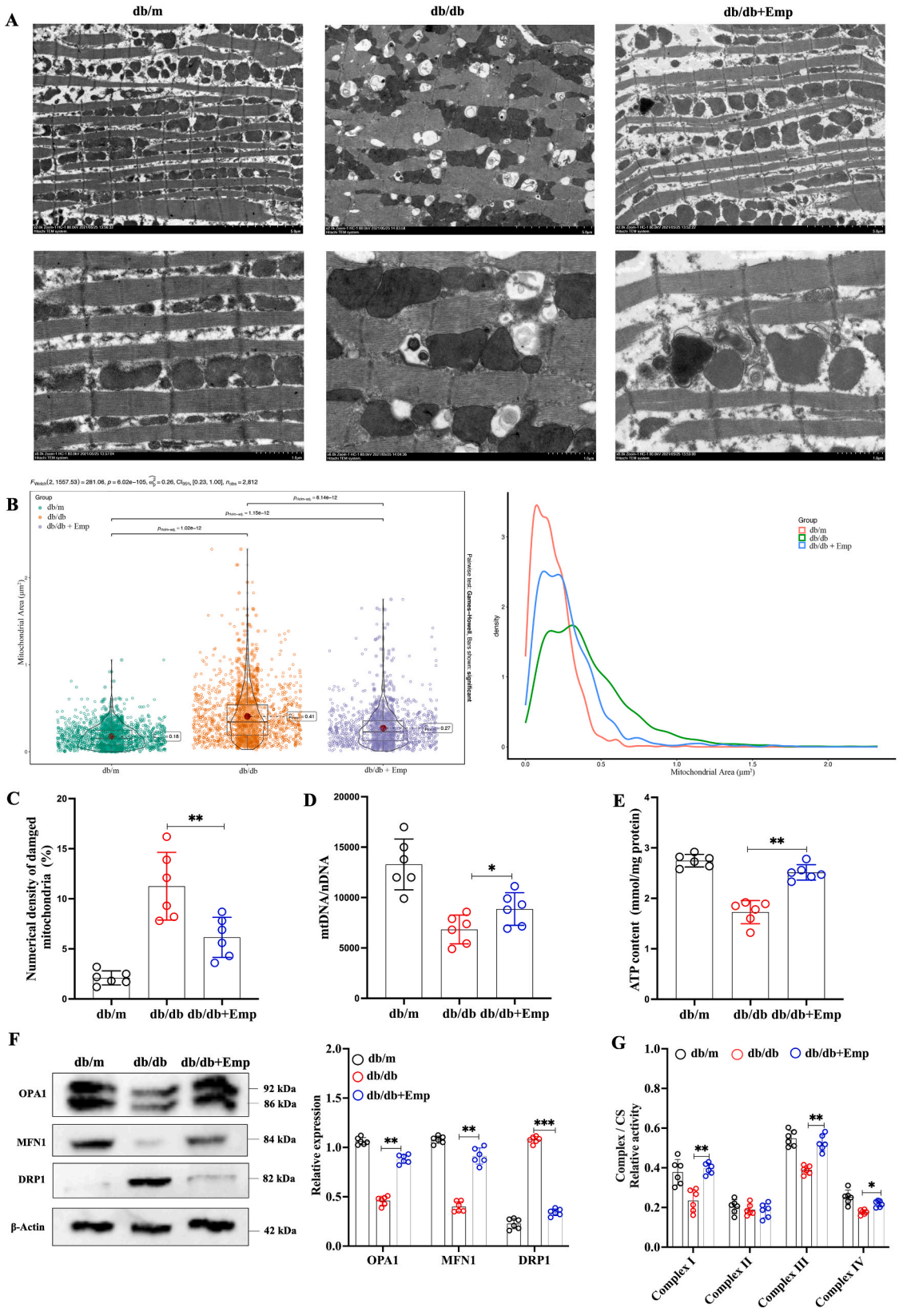

Fig. 9. Emp ameliorates cardiac mitochondrial dysfunction in db/db mice. (A) Representative transmission electron microscopy images of cardiac mitochondria from each group of mice. (B) Quantitative analysis of mitochondrial area and mitochondrial volume density in the heart of each group of mice. (C) Percentage value densities of myocardial mitochondrial damage in each group. (D) Number of mtDNA copies of each nuclear genome in cardiac tissues. n = 6. (E) ATP content in cardiac tissues. (F) Western blot analysis of the expression of mitochondrial kinetic markers MFN1, OPA1 and DRP1 in cardiac tissues. n = 6. (G) Mitochondrial electron transport chain complex activity data for each group. Mean ± SD indicated, n = 6. $^{*}P < 0.05$, $^{**}P < 0.01$, $^{***}P < 0.001$.

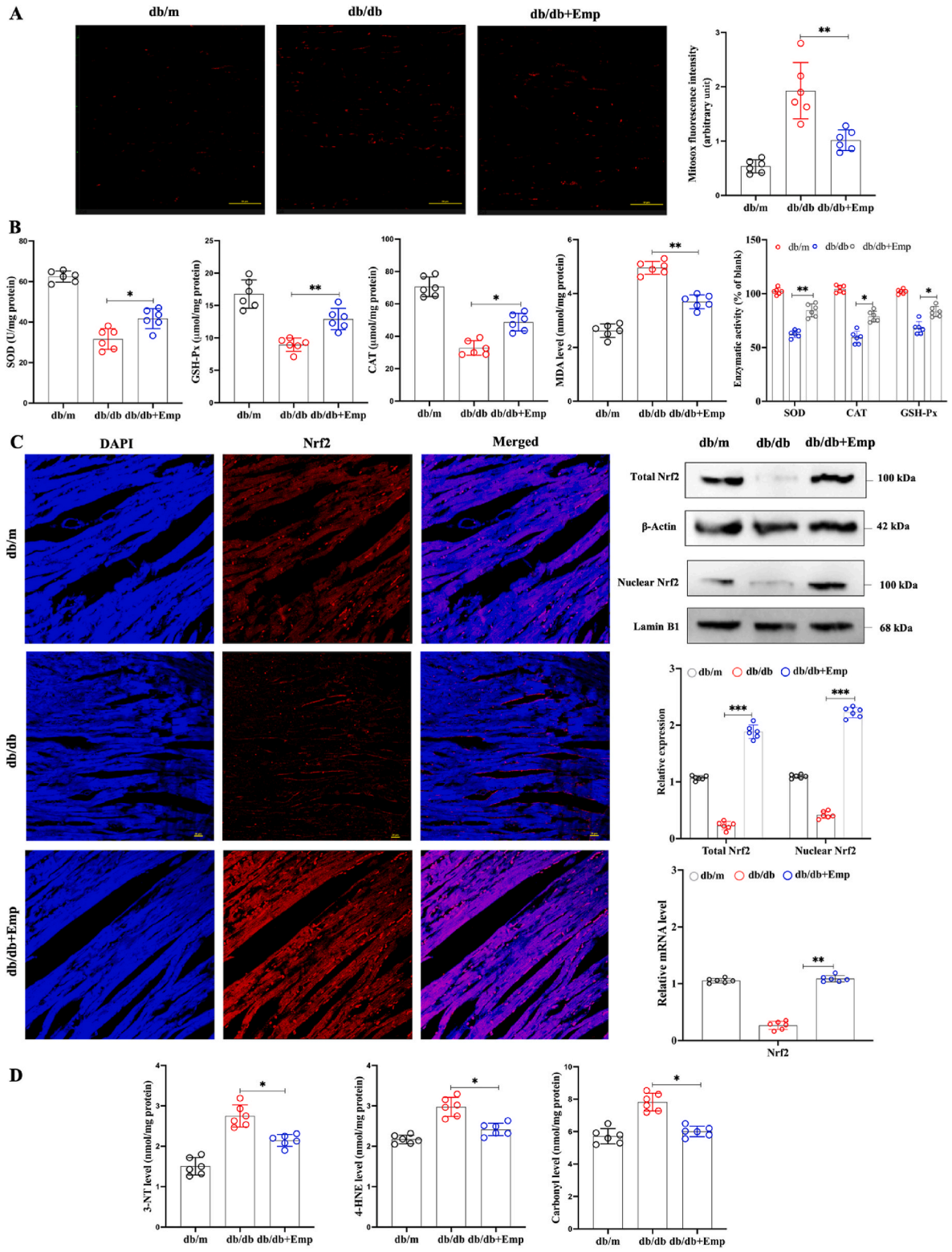

Fig. 10. Emp improves intracellular oxidative stress in cardiomyocytes of db/db mice. (A) Quantitative and representative images of MitoSox fluorescence intensity in cardiac tissues of each group of mice, scale bar = 50 μm, n = 6. (B) ELISA for the detection of SOD, GSH-Px, CAT and MDA content and enzyme activities in mouse heart tissues, n = 6. (C) Immunofluorescence, western and qRT-PCR were performed to detect the levels of Nrf2 protein and mRNA. Scale bar = 20 μm. (D) Levels of markers of oxidative damage, 3-NT, 4-HNE and carbocycline were detected. Data are expressed as mean ± SD, n = 6. $^{*}P < 0.05$, $^{**}P < 0.01$, $^{***}P < 0.001$.

levels of BDH1 and OXCT1, whereas the expression of HMGCS2 remained unchanged (Fig. 11A). Moreover, in agreement with the results of the in vivo experiments, there was a significant improvement after Emp treatment, and SOD, GSH-Px and CAT enzyme activities were elevated, while MDA levels were significantly decreased (Fig. 11B and C). We assessed ROS production in HG-stimulated cultured H9C2 cells and found that treatment with Emp resulted in reduced cellular ROS production (Fig. 11D and E). In addition, immunofluorescence

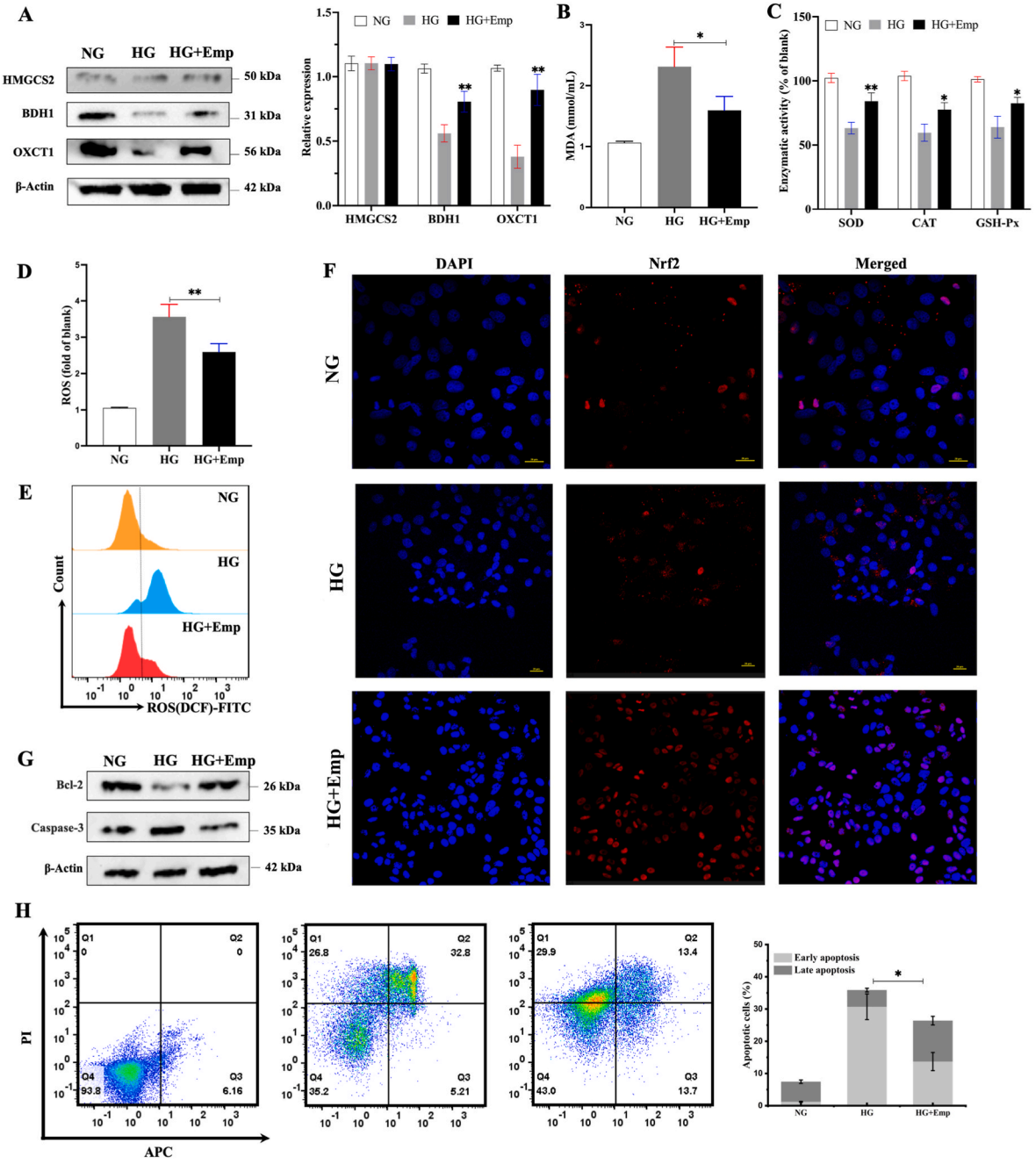

Fig. 11. Effects of Emp on HG-induced ketolysis enzymes, oxidative stress and apoptosis of cardiomyocytes. (A) Western blot analysis of representative expression of HMGCS2, BDH1 and OXCT1 proteins in each group of H9C2 cells, with β-actin as loading control. (B) Detection of MDA levels. (C) Detection of SOD, GSH-Px and CAT enzyme activities. (D) Detection of intracellular ROS levels using ROS detection kit. (E) DCF-FITC/count waterfall image, a representative picture of ROS produced in H9C2 cells measured by flow cytometry using DCFH-DA probe. (F) Immunofluorescence detection of fluorescence intensity of Nrf2 in H9C2 cells of each group, scale bar = 20 μm. (G) Western blotting analysis of representative expression of Caspase-3 and Bcl-2 proteins in H9C2 cells of each group, β-actin was used as loading control. (F) Flow cytometry was used to measure the apoptosis level of H9C2 cells in each group. The data were expressed as mean ± SD, n = 3. $^{*}P < 0.05$, $^{**}P < 0.01$.

technique to localise the translocation of Nrf2 protein in the cells showed that the cells in the Emp + HG group showed hyperfluorescence in the nucleus, and both Nrf2 expression was increased, and nuclear translocation took place, compared to the HG group (Fig. 11F). We also detected the downstream cell protection related genes of Nrf2 pathway. As shown in Fig. S3, mRNA expression levels of genes related to the Nrf2 pathway were significantly higher than those in the HG group after Emp administration. Excessive oxidative stress was closely related to the induction of apoptosis, and Bcl-2 expression was increased and Caspase-3 expression was decreased in db/db mice treated with Emp compared with the db/db group (Fig. 11G), and flow cytometry assay also showed that apoptosis of cardiomyocytes was significantly attenuated in the Emp + HG group (Fig. 11H).

4. Discussion

In our study, we used a high-throughput gene expression database to analyze 9 gene expression datasets in DCM. R-packet RobustRankAggreg was used to achieve the final expression analysis of nine different chips, and the most significantly upregulated gene was HMGCS2. Significantly

down-regulated genes include BDH1 and the rate-limiting ketolysis enzyme OXCT1. In addition, based on the analysis of the constructed protein interaction network, it was found that HMGCS2 was in the core position of the interaction network. GO enrichment analysis mainly focused on several molecular function items such as REDOX process, catalytic activity, REDOX enzyme activity, mitochondria and peroxisome. The enrichment analysis of KEGG pathway included peroxisome, metabolic pathway and PPAR signaling pathway. The results of GSEA analysis showed that differential genes were mainly involved in the PPAR signaling pathway, and the importance of this signaling pathway in the pathogenesis of DCM and ketone body metabolism has been reported in related literature [29]. Combining GO, KEGG, GSEA analysis and PPI network construction, we selected HMGCS2, the key synthetase of ketone body metabolism pathway, and BDH1 and OXCT1 as the key ketolysis molecules to study.

The traditional view is that the liver synthesizes ketone bodies, but our study found that the DCM heart is also involved in ketone body synthesis catabolism. We detected key enzymes of ketone body metabolism at 8, 12 and 16 weeks of db/db respectively, and found that the expression of ketone body synthetase HMGCS2 significantly increased, and the expression levels of key mitochondrial ketolytic enzymes OXCT1 and BDH1 decreased, both at protein level and mRNA level. In vitro experiments, we found that the expression levels of OXCT1 and BDH1 in cardiomyocytes induced by HG were significantly decreased, and the above results were consistent with the results of the high-throughput gene expression database, but no significant changes were found in the expression of HMGCS2 in cardiomyocytes induced by high sugar. Combined with other published findings, the expression of ketogenic enzyme HMGCS2 in cardiomyocytes may not be related to the increase of glucose [13]. However, the increase of glucose can inhibit the ketone dissolution ability of the heart, suggesting that there is crosstalk between glucose and ketone body metabolism in diabetic myocardium. Inhibition of myocardial HMGCS2 reduces β-OHB accumulation and improves functional recovery during reperfusion [4]. Heart-specific deletion models encoding the BDH1 and OXCT1 genes [14,30] have been produced, and BDH1 knockout mice can develop cardiac dysfunction after prolonged fasting. In addition, BDH1 and OXCT1 knockout mice worsened heart failure after ischemia compared to wild-type mice. We also found elevated β-OHB levels in heart muscle, serum, and urine, while AcAc levels were also elevated, indicating an imbalance in the availability and utilization of ketone bodies. These studies suggest that decreased ketone oxidation may be a marker of DCM. Based on sequencing analysis combined with our study, ketone metabolism does not play an adaptive role in promoting normal cardiac function and slowing disease progression in DCM. Although the expression of ketone body synthetase HMGCS2 is increased in myocardium, the catabolic ketone bodies cannot be converted into energy due to the decreased expression levels and activity of the ketolysis enzymes BDH1 and OXCT1, and cardiomyocytes produce more negative feedback ketone bodies. This vicious cycle can aggravate myocardial energy deficiency, damage cardiomyocytes, and further aggravate cardiomyopathy.

A large body of evidence-based evidence has confirmed that SGLT2i has cardiac benefits in patients with diabetes and may reduce the risk of adverse cardiac events even in patients with heart failure without diabetes. This study found that compared with db/db group, db/db + Emp group can reduce fasting and random blood glucose levels, reduce body weight, and improve cardiac function related indicators. In addition, it can reduce myocardial hypertrophy and myocardial fibrosis, and reduce myocardial cell apoptosis. SGLT2i can induce mild ketosis. In combination with the abnormal expression of key enzymes of ketone metabolism in DCM found in this study, we want to investigate whether SGLT2i can provide energy for diabetic myocardium by inducing mild ketosis, and thus benefit cardiovascular diseases. Verma S et al. showed that Emp increased myocardial energy production in db/db mice [12]. We indeed found that Emp further promoted the activity of BDH1 and OXCT1, increased the utilization of ketone bodies, further promoted the activity of HMGCS2 enzyme in DCM heart, increased the synthesis of ketone bodies, formed a virtuous cycle, and removed the upstream traffic congestion (ketone bodies cannot be broken down and utilized). whereas similar results were not found in high-glucose-induced cardiomyocytes. The differences in the above results consider the presence of cardioprotective effect of β-OHB in in vivo experiments. In the in vitro experiments of the present study, however, no cardiomyocytes were treated with β-OHB in the presence of high glucose induction. β-OHB is no longer a single metabolic intermediate and acts as an endogenous signaling molecule, functioning as a stress molecule [31]. It has been reported that βOHB improved cell viability, reduced ROS production and ameliorated mitochondrial dysfunction in Dox-treated H9C2 cells [32]. Furthermore, exogenous βOHB infusion protected against cardiac ischemic injury by reducing ROS and enhancing ATP production [33]. Finally, the positive effects of Emp on key ketone body synthases and catabolic enzymes, especially catabolic enzymes in alleviating DCM, should also be considered. The main problem associated with the DM heart may be the low energy utilization due to low catabolic utilization of ketone bodies [3,13,34,35], but further in-depth molecular mechanistic studies are needed.

It is well known that ketone bodies are catabolic in the mitochondrial matrix, and the large amount of ATP produced by the mitochondria is essential for the play of cardiac function [36]. In diabetes, impaired mitochondrial homeostasis leads to abnormal ketone metabolism, which in turn obstructs ATP production. In this study, through myocardial transmission electron microscopy, it was found that db/db + Emp group improved the structural aberrations such as mitochondrial swelling and ridge breakage, and the mitochondrial area and volume density were reduced. In addition, after Emp treatment, the damage degree of mitochondrial electron transport chain was significantly improved, and the expression of MFN1 and OPA1 of mitochondrial fusion markers was up-regulated, while the expression of DRP1 of mitochondrial division markers was down-regulated, thereby improving mitochondrial dysfunction, increasing ATP levels in myocardial tissue, restoring energy metabolism, and providing more energy to cardiomyocytes [12,37,38].

Oxidative stress of cardiomyocytes is one of the main factors in the pathogenesis of DCM. SGLT2i has also been shown to play a key role in reducing oxidative stress in DCM, unrelated to hypoglycemic effects [39,40]. We evaluated ROS production in diabetic hearts and found that after treatment with Emp, mitochondrial ROS production decreased, while antioxidant enzymes SOD, GSH-Px and CAT enzyme activity increased, and MDA levels decreased. In addition, Nrf2 is a major regulator of anti-oxidative stress. Our study found that Emp can promote Nrf2 transport to the nucleus, and the mRNA expression level of downstream genes of Nrf2 pathway after Emp treatment is significantly higher than that of HG group. Several previous studies have shown that Nrf2 deletion is related to cellular stress damage in diabetic animal models, and Emp can activate Nrf2/ARE signaling, thereby inhibiting myocardial oxidative stress [21,41,42]. These studies suggest that Emp can be used as a drug targeting Nrf2 signaling pathway to reduce oxidative stress in DCM. We also found that Emp treatment significantly weakened the levels of 3-NT, 4-HNE and carbonyl, markers of oxidative damage. Oxidative stress can lead to cardiomyocyte injury and apoptosis, which is consistent with our previous in vivo experiments and other study, Emp treatment can inhibit myocardial tissue or HG-induced apoptosis [43]. These results suggest that Emp can reduce oxidative stress and myocardial cell apoptosis in diabetic heart.

In conclusion, the aim of this study was to observe the changes of key enzymes of keto body metabolism and oxidative stress in the early stage of DCM, and regulate keto body metabolism by Emp treatment, so as to improve mitochondrial dysfunction in diabetic cardiomyopathy. These findings provide a theoretical basis for evaluating Emp as a treatment for DCM patients. Subsequent studies will further observe the changes of key enzymes of ketone metabolism and key pathways of anti-oxidative stress during advanced DCM, as well as the role of β-hydroxybutyric

acid as a stress molecule in DCM, so as to obtain more evidence of the benefits of Emp in improving myocardial ketone metabolism and oxidative stress.

Funding

This work was supported by the Medical Science and Technology Research Fund of Guangdong Province (A2023277) and Central People's Hospital of Zhanjiang Startup Project of Doctor Scientific Research (2022A23 and 2022A26).

CRediT authorship contribution statement

Weijuan Cai: Data curation, Formal analysis, Funding acquisition, Investigation, Methodology, Resources, Software, Writing – original draft. **Kunying Chong:** Data curation, Investigation, Methodology. **Yunfei Huang:** Investigation, Resources. **Chun Huang:** Data curation, Resources. **Liang Yin:** Conceptualization, Data curation, Formal analysis, Funding acquisition, Project administration, Resources, Software, Supervision, Validation, Visualization, Writing – review & editing.

Declaration of competing interest

The authors declare that they have no known competing financial interests or personal relationships that could have appeared to influence the work reported in this paper.

Data availability

No data was used for the research described in the article.

Appendix A. Supplementary data

Supplementary data to this article can be found online at https://doi.org/10.1016/j.redox.2023.103010.

References

[1] I.G. Poornima, P. Parikh, R.P. Shannon, Diabetic cardiomyopathy: the search for a unifying hypothesis, Circ. Res. 98 (2006) 596–605.
[2] D.G. Cotter, R.C. Schugar, P.A. Crawford, Ketone body metabolism and cardiovascular disease, Am. J. Physiol. Heart Circ. Physiol. 304 (2013) H1060–H1076.
[3] H.B. Kang, J. Fan, R. Lin, S. Elf, Q. Ji, L. Zhao, L. Jin, J.H. Seo, C. Shan, J.L. Arbiser, C. Cohen, D. Brat, H.M. Miziorko, E. Kim, O. Abdel-Wahab, T. Merghoub, S. Frohling, C. Scholl, P. Tamayo, D.A. Barbie, L. Zhou, B.P. Pollack, K. Fisher, R. R. Kudchadkar, D.H. Lawson, G. Sica, M. Rossi, S. Lonial, H.J. Khoury, F.R. Khuri, B.H. Lee, T.J. Boggon, C. He, S. Kang, J. Chen, Metabolic rewiring by oncogenic BRAF V600E links ketogenesis pathway to BRAF-MEK1 signaling, Mol. Cell. 59 (2015) 345–358.
[4] R.T. Lindsay, S. Dieckmann, D. Krzyzanska, D. Manetta-Jones, J.A. West, C. Castro, J.L. Griffin, A.J. Murray, beta-hydroxybutyrate accumulates in the rat heart during low-flow ischaemia with implications for functional recovery, Elife 10 (2021).
[5] D. Zhang, H. Yang, X. Kong, K. Wang, X. Mao, X. Yan, Y. Wang, S. Liu, X. Zhang, J. Li, L. Chen, J. Wu, M. Wei, J. Yang, Y. Guan, Proteomics analysis reveals diabetic kidney as a ketogenic organ in type 2 diabetes, Am. J. Physiol. Endocrinol. Metab. 300 (2011) E287–E295.
[6] C. Le Foll, A.A. Dunn-Meynell, H.M. Miziorko, B.E. Levin, Regulation of hypothalamic neuronal sensing and food intake by ketone bodies and fatty acids, Diabetes 63 (2014) 1259–1269.
[7] Y. Nonaka, T. Takagi, M. Inai, S. Nishimura, S. Urashima, K. Honda, T. Aoyama, S. Terada, Lauric acid stimulates ketone body production in the KT-5 astrocyte cell line, J. Oleo Sci. 65 (2016) 693–699.
[8] M. El Azzouny, M.J. Longacre, I.H. Ansari, R.T. Kennedy, C.F. Burant, M. J. MacDonald, Knockdown of ATP citrate lyase in pancreatic beta cells does not inhibit insulin secretion or glucose flux and implicates the acetoacetate pathway in insulin secretion, Mol. Metabol. 5 (2016) 980–987.
[9] J. Adijanto, J. Du, C. Moffat, E.L. Seifert, J.B. Hurle, N.J. Philp, The retinal pigment epithelium utilizes fatty acids for ketogenesis, J. Biol. Chem. 289 (2014) 20570–20582.
[10] D. Chen, X. Ruan, Y. Liu, Y. He, HMGCS2 silencing attenuates high glucose-induced in vitro diabetic cardiomyopathy by increasing cell viability, and inhibiting apoptosis, inflammation, and oxidative stress, Bioengineered 13 (2022) 11417–11429.
[11] S.K. Shukla, W. Liu, K. Sikder, S. Addya, A. Sarkar, Y. Wei, K. Rafiq, HMGCS2 is a key ketogenic enzyme potentially involved in type 1 diabetes with high cardiovascular risk, Sci. Rep. 7 (2017) 4590.
[12] S. Verma, S. Rawat, K.L. Ho, C.S. Wagg, L. Zhang, H. Teoh, J.E. Dyck, G.M. Uddin, G.Y. Oudit, E. Mayoux, M. Lehrke, N. Marx, G.D. Lopaschuk, Empagliflozin increases cardiac energy production in diabetes: novel translational insights into the heart failure benefits of SGLT2 inhibitors, JACC Basic Transl Sci 3 (2018) 575–587.
[13] M.K. Brahma, C.M. Ha, M.E. Pepin, S. Mia, Z. Sun, J.C. Chatham, K.M. Habegger, E. D. Abel, A.J. Paterson, M.E. Young, A.R. Wende, Increased glucose availability attenuates myocardial ketone body utilization, J. Am. Heart Assoc. 9 (2020), e013039.
[14] R.C. Schugar, A.R. Moll, D. Andre d'Avignon, C.J. Weinheimer, A. Kovacs, P. A. Crawford, Cardiomyocyte-specific deficiency of ketone body metabolism promotes accelerated pathological remodeling, Mol. Metabol. 3 (2014) 754–769.
[15] B. Zinman, C. Wanner, J.M. Lachin, D. Fitchett, E. Bluhmki, S. Hantel, M. Mattheus, T. Devins, O.E. Johansen, H.J. Woerle, U.C. Broedl, S.E. Inzucchi, E.-R. O. Investigators, Empagliflozin, cardiovascular outcomes, and mortality in type 2 diabetes, N. Engl. J. Med. 373 (2015) 2117–2128.
[16] M. Packer, J. Butler, F. Zannad, G. Filippatos, J.P. Ferreira, S.J. Pocock, P. Carson, I. Anand, W. Doehner, M. Haass, M. Komajda, A. Miller, S. Pehrson, J.R. Teerlink, S. Schnaidt, C. Zeller, J.M. Schnee, S.D. Anker, Effect of empagliflozin on worsening heart failure events in patients with heart failure and preserved ejection fraction: EMPEROR-preserved trial, Circulation 144 (2021) 1284–1294.
[17] S. Verma, N.K. Dhingra, J. Butler, S.D. Anker, J.P. Ferreira, G. Filippatos, J. L. Januzzi, C.S.P. Lam, N. Sattar, B. Peil, M. Nordaby, M. Brueckmann, S.J. Pocock, F. Zannad, M. Packer, E.M.-R.t. committees, investigators, Empagliflozin in the treatment of heart failure with reduced ejection fraction in addition to background therapies and therapeutic combinations (EMPEROR-Reduced): a post-hoc analysis of a randomised, double-blind trial, Lancet Diabetes Endocrinol. 10 (2022) 35–45.
[18] S.D. Wiviott, I. Raz, M.P. Bonaca, O. Mosenzon, E.T. Kato, A. Cahn, M. G. Silverman, T.A. Zelniker, J.F. Kuder, S.A. Murphy, D.L. Bhatt, L.A. Leiter, D. K. McGuire, J.P.H. Wilding, C.T. Ruff, I.A.M. Gause-Nilsson, M. Fredriksson, P. A. Johansson, A.M. Langkilde, M.S. Sabatine, D.-T. Investigators, Dapagliflozin and cardiovascular outcomes in type 2 diabetes, N. Engl. J. Med. 380 (2019) 347–357.
[19] Q.G. Karwi, D. Biswas, T. Pulinilkunnil, G.D. Lopaschuk, Myocardial ketones metabolism in heart failure, J. Card. Fail. 26 (2020) 998–1005.
[20] S. Verma, J.J.V. McMurray, SGLT2 inhibitors and mechanisms of cardiovascular benefit: a state-of-the-art review, Diabetologia 61 (2018) 2108–2117.
[21] C. Li, J. Zhang, M. Xue, X. Li, F. Han, X. Liu, L. Xu, Y. Lu, Y. Cheng, T. Li, X. Yu, B. Sun, L. Chen, SGLT2 inhibition with empagliflozin attenuates myocardial oxidative stress and fibrosis in diabetic mice heart, Cardiovasc. Diabetol. 18 (2019) 15.
[22] S.D. Anker, J. Butler, G. Filippatos, J.P. Ferreira, E. Bocchi, M. Bohm, H.P. Brunner-La Rocca, D.J. Choi, V. Chopra, E. Chuquiure-Valenzuela, N. Giannetti, J.E. Gomez-Mesa, S. Janssens, J.L. Januzzi, J.R. Gonzalez-Juanatey, B. Merkely, S.J. Nicholls, S.V. Perrone, I.L. Pina, P. Ponikowski, M. Senni, D. Sim, J. Spinar, I. Squire, S. Taddei, H. Tsutsui, S. Verma, D. Vinereanu, J. Zhang, P. Carson, C.S.P. Lam, N. Marx, C. Zeller, N. Sattar, W. Jamal, S. Schnaidt, J.M. Schnee, M. Brueckmann, S.J. Pocock, F. Zannad, M. Packer, E.M.-P.T. Investigators, Empagliflozin in heart failure with a preserved ejection fraction, N. Engl. J. Med. 385 (2021) 1451–1461.
[23] S.D. Solomon, J.J.V. McMurray, B. Claggett, R.A. de Boer, D. DeMets, A. F. Hernandez, S.E. Inzucchi, M.N. Kosiborod, C.S.P. Lam, F. Martinez, S.J. Shah, A. S. Desai, P.S. Jhund, J. Belohlavek, C.E. Chiang, C.J.W. Borleffs, J. Comin-Colet, D. Dobreanu, J. Drozdz, J.C. Fang, M.A. Alcocer-Gamba, W. Al Habeeb, Y. Han, J. W. Cabrera Honorio, S.P. Janssens, T. Katova, M. Kitakaze, B. Merkely, E. O'Meara, J.F.K. Saraiva, S.N. Tereshchenko, J. Thierer, M. Vaduganathan, O. Vardeny, S. Verma, V.N. Pham, U. Wilderang, N. Zaozerska, E. Bachus, D. Lindholm, M. Petersson, A.M. Langkilde, D.T. Committees, Investigators, Dapagliflozin in heart failure with mildly reduced or preserved ejection fraction, N. Engl. J. Med. 387 (2022) 1089–1098.
[24] Z. Wang, K. Chen, Y. Han, H. Zhu, X. Zhou, T. Tan, J. Zeng, J. Zhang, Y. Liu, Y. Li, Y. Yao, J. Yi, D. He, J. Zhou, J. Ma, C. Zeng, Irisin protects heart against ischemia-reperfusion injury through a SOD2-dependent mitochondria mechanism, J. Cardiovasc. Pharmacol. 72 (2018) 259–269.
[25] A.E. Wentz, D.A. d'Avignon, M.L. Weber, D.G. Cotter, J.M. Doherty, R. Kerns, R. Nagarajan, N. Reddy, N. Sambandam, P.A. Crawford, Adaptation of myocardial substrate metabolism to a ketogenic nutrient environment, J. Biol. Chem. 285 (2010) 24447–24456.
[26] M.E. Young, R.A. Brewer, R.A. Peliciari-Garcia, H.E. Collins, L. He, T.L. Birky, B. W. Peden, E.G. Thompson, B.J. Ammons, M.S. Bray, J.C. Chatham, A.R. Wende, Q. Yang, C.W. Chow, T.A. Martino, K.L. Gamble, Cardiomyocyte-specific BMAL1 plays critical roles in metabolism, signaling, and maintenance of contractile function of the heart, J. Biol. Rhythm. 29 (2014) 257–276.
[27] Y. Ikeda, A. Shirakabe, Y. Maejima, P. Zhai, S. Sciarretta, J. Toli, M. Nomura, K. Mihara, K. Egashira, M. Ohishi, M. Abdellatif, J. Sadoshima, Endogenous Drp1 mediates mitochondrial autophagy and protects the heart against energy stress, Circ. Res. 116 (2015) 264–278.
[28] S.R. Yurista, H.H.W. Sillje, S.U. Oberdorf-Maass, E.M. Schouten, M.G. Pavez Giani, J.L. Hillebrands, H. van Goor, D.J. van Veldhuisen, R.A. de Boer, B.D. Westenbrink, Sodium-glucose co-transporter 2 inhibition with empagliflozin improves cardiac function in non-diabetic rats with left ventricular dysfunction after myocardial infarction, Eur. J. Heart Fail. 21 (2019) 862–873.
[29] S. Zhang, C. Xie, The role of OXCT1 in the pathogenesis of cancer as a rate-limiting enzyme of ketone body metabolism, Life Sci. 183 (2017) 110–115.

[30] J.L. Horton, M.T. Davidson, C. Kurishima, R.B. Vega, J.C. Powers, T.R. Matsuura, C. Petucci, E.D. Lewandowski, P.A. Crawford, D.M. Muoio, F.A. Recchia, D.P. Kelly, The failing heart utilizes 3-hydroxybutyrate as a metabolic stress defense, JCI Insight (2019) 4.
[31] P. Rojas-Morales, J. Pedraza-Chaverri, E. Tapia, Ketone bodies, stress response, and redox homeostasis, Redox Biol. 29 (2020), 101395.
[32] C.M. Oh, S. Cho, J.Y. Jang, H. Kim, S. Chun, M. Choi, S. Park, Y.G. Ko, Cardioprotective potential of an SGLT2 inhibitor against doxorubicin-induced heart failure, Korean Circ J 49 (2019) 1183–1195.
[33] Y. Yu, Y. Yu, Y. Zhang, Z. Zhang, W. An, X. Zhao, Treatment with D-beta-hydroxybutyrate protects heart from ischemia/reperfusion injury in mice, Eur. J. Pharmacol. 829 (2018) 121–128.
[34] P.K. Mishra, Why the diabetic heart is energy inefficient: a ketogenesis and ketolysis perspective, Am. J. Physiol. Heart Circ. Physiol. 321 (2021) H751–H755.
[35] Y. Mizuno, E. Harada, H. Nakagawa, Y. Morikawa, M. Shono, F. Kugimiya, M. Yoshimura, H. Yasue, The diabetic heart utilizes ketone bodies as an energy source, Metabolism 77 (2017) 65–72.
[36] S.B. Ong, S.B. Kalkhoran, H.A. Cabrera-Fuentes, D.J. Hausenloy, Mitochondrial fusion and fission proteins as novel therapeutic targets for treating cardiovascular disease, Eur. J. Pharmacol. 763 (2015) 104–114.
[37] A. Baartscheer, C.A. Schumacher, R.C. Wust, J.W. Fiolet, G.J. Stienen, R. Coronel, C.J. Zuurbier, Empagliflozin decreases myocardial cytoplasmic Na(+) through inhibition of the cardiac Na(+)/H(+) exchanger in rats and rabbits, Diabetologia 60 (2017) 568–573.
[38] M. Packer, SGLT2 inhibitors: role in protective reprogramming of cardiac nutrient transport and metabolism, Nat. Rev. Cardiol. 20 (2023) 443–462.
[39] B. Lin, N. Koibuchi, Y. Hasegawa, D. Sueta, K. Toyama, K. Uekawa, M. Ma, T. Nakagawa, H. Kusaka, S. Kim-Mitsuyama, Glycemic control with empagliflozin, a novel selective SGLT2 inhibitor, ameliorates cardiovascular injury and cognitive dysfunction in obese and type 2 diabetic mice, Cardiovasc. Diabetol. 13 (2014) 148.
[40] M. Xue, T. Li, Y. Wang, Y. Chang, Y. Cheng, Y. Lu, X. Liu, L. Xu, X. Li, X. Yu, B. Sun, L. Chen, Empagliflozin prevents cardiomyopathy via sGC-cGMP-PKG pathway in type 2 diabetes mice, Clin. Sci. (Lond.) 133 (2019) 1705–1720.
[41] M.S. Bitar, F. Al-Mulla, A defect in Nrf2 signaling constitutes a mechanism for cellular stress hypersensitivity in a genetic rat model of type 2 diabetes, Am. J. Physiol. Endocrinol. Metab. 301 (2011) E1119–E1129.
[42] J.L. Zweier, P. Kuppusamy, G.A. Lutty, Measurement of endothelial cell free radical generation: evidence for a central mechanism of free radical injury in postischemic tissues, Proc. Natl. Acad. Sci. U. S. A. 85 (1988) 4046–4050.
[43] S.A.G. Eltobshy, R. Messiha, E. Metias, M. Sarhan, R. El-Gamal, A. El-Shaieb, M. Ghalwash, Effect of SGLT2 inhibitor on cardiomyopathy in a rat model of T2DM: possible involvement of cardiac aquaporins, Tissue Cell 85 (2023), 102200.